Asian Journal of Chemical Sciences

Volume 13, Issue 6, Page 13-38, 2023; Article no.AJOCS.107181
ISSN: 2456-7795

Baobab (*Adansonia digitata*) Pulp and Mango Seeds as New Adsorbents for the Removal of Pb (II) Ions from Aqueous Solutions

Rome Kenneth [a], Kalu M. Kalu [b*], Naibi A. Haruna [c], Emmanuel K. Chinedu [d], Ismaila Atiku [c] and Michael Emmanuel [b,e]

[a] Department of Chemistry, University of Ilorin, PMB 1515, Ilorin, Nigeria.
[b] Department of Chemistry, Gombe State University, P.M.B. 127, Tudun Wada, Gombe, Gombe State, Nigeria.
[c] Department of Chemistry, Adamawa State College of Agriculture, Ganye, Adamawa State, Nigeria.
[d] Department of Chemistry, Modibbo Adama University, Yola, Adamawa State, Nigeria.
[e] Department of Chemistry, Saint Louis University, 3501 Laclede Ave, St. Louis, MO 63103, USA.

Authors' contributions

This work was carried out in collaboration among all authors. All authors read and approved the final manuscript.

Article Information

DOI: 10.9734/AJOCS/2023/v13i6260

Open Peer Review History:
This journal follows the Advanced Open Peer Review policy. Identity of the Reviewers, Editor(s) and additional Reviewers, peer review comments, different versions of the manuscript, comments of the editors, etc are available here: https://www.sdiarticle5.com/review-history/107181

Original Research Article

Received: 02/08/2023
Accepted: 04/10/2023
Published: 07/10/2023

ABSTRACT

Baobab pulp (Adansonia digitata) and mango seeds were employed in the synthesis of activated carbon, serving as a cost-efficient adsorbent for the elimination of Pb (II) ions from aqueous solutions. The carbonization of baobab pulp and mango seeds was executed within a muffle furnace at 500°C for 2 hours and 30 minutes, followed by activation using orthophosphoric acid.

**Corresponding author: E-mail: michaelkalu14@gmail.com;*

Batch adsorption experiments encompassed assessments of initial metal ion concentration, adsorbent dosage, contact time, pH, and temperature, aimed at optimizing conditions to achieve maximal adsorption. The maximum monolayer adsorption capacities for Pb(II) were determined as 18.69 mg/g for Baobab activated carbon (BAC) and 16.02 mg/g for Mango seed activated carbon (MAC) at a concentration of 500 mg/l.

Adsorption data were subjected to analysis using Langmuir, Freundlich, and Temkin isotherm models. Among these models, Langmuir exhibited superior fit, as indicated by a correlation coefficient (R^2) exceeding 0.99. Kinetic evaluation encompassed Pseudo-first-order, Pseudo-second-order, and Intra-particle diffusion models, with the Pseudo-second-order model emerging as the most appropriate. This finding suggests that the adsorption process is primarily governed by chemisorption, potentially serving as the rate-limiting step.

Thermodynamic investigations revealed the spontaneity, endothermic nature, and heightened randomness at the solid-solution interface of the adsorption process. Further assessment involved desorption experiments to ascertain the reusability and lifespan of the adsorbents. The outcomes underscore the potential of activated carbon derived from baobab pulp and mango seeds as economical and efficient adsorbents for Pb (II) ion removal.

Keywords: Activated carbon; baobab pulp; Pb(II) Ions; adsorption isotherms; kinetics; thermodynamics.

1. INTRODUCTION

Water pollution caused by technological development remains a significant and pressing concern. The escalating production of heavy metals through technological processes has led to elevated metal concentrations in aquatic environments, surpassing established water quality thresholds crucial for safeguarding ecosystems, wildlife, and human health. The primary industries responsible for releasing metal-laden wastewater include mining, mineral processing, pigment manufacturing, the painting and photographic sectors, as well as metalworking and finishing operations [1]. These metals primarily encompass elements located within the d-block of the periodic table, commonly referred to as transition metals [2].

Of note among these hazardous metals is lead, a toxic heavy metal that holds substantial environmental and occupational implications. Ranking second on the list of prioritized hazardous materials, lead's perilous nature becomes evident even in minute quantities. Its ingress into the human body occurs through multiple avenues. Inhalation of dust containing lead-based paints or exhaust emissions from leaded gasoline is one route. Additionally, trace amounts are present in various foods, notably fish, which are disproportionately affected by industrial pollution. Furthermore, aging residences may still have lead water pipes, subsequently tainting drinking water through the gradual dissolution of the lead pipes. Although a substantial proportion of ingested lead is excreted through urine, the risk of accumulation remains, particularly among children [3]. The adverse effects of lead exposure are cumulative over time. Elevated levels of lead within the body can culminate in fatality or enduring damage to critical systems such as the central nervous system, brain, and kidneys [4]. This resultant impairment frequently manifests as behavioral and cognitive disorders (including hyperactivity), memory and concentration deficits, hypertension, auditory impairments, headaches, stunted growth, fertility issues in both genders, gastrointestinal disturbances, as well as muscular and articular discomfort.

“Extensive research has been conducted on lead due to its deleterious consequences. Lead forms intricate complexes with oxo-groups within enzymes, thereby influencing virtually all stages of hemoglobin synthesis and porphyrin metabolism” [5].

“Due to the aforementioned factors, a compelling imperative exists to mitigate the presence of these metals within wastewater, thereby averting the contamination of natural water bodies through the discharge of deleterious metal-laden effluents. Traditional approaches for the extraction of heavy metal ions from industrial wastewater encompass a range of methodologies, including chemical precipitation, oxidation, reduction, reverse osmosis, membrane filtration, electro-dialysis, solvent extraction, electro-coagulation, and adsorption. However, these techniques are not without inherent constraints, such as demanding operational

parameters, suboptimal metal removal efficacy, and the generation of secondary sludge that entails substantial disposal costs" [6].

Among the array of methodologies mentioned above, the most auspicious solution for effectuating the removal of metal ions from industrial effluents emerges in the form of adsorption. This approach exhibits unparalleled promise, primarily due to the capacity for the employed adsorbent material to undergo rejuvenating desorption processes, rendering it eminently reusable, efficient, and economically viable [7].

Activated carbon stands as the predominant and widely employed adsorbent in the realm of adsorption, lauded for its remarkable efficacy and adaptability [8], [9]. Distinguished by its extensive porosity, substantial internal surface area, and commendable mechanical robustness, activated carbon holds a significant position. However, it is worth noting that despite its prevalent usage across industries, activated carbon remains a cost-intensive material.

The escalating interest in harnessing agricultural-derived precursors for the synthesis of activated carbon finds its roots in multifaceted advantages. This approach is notably driven by the economic viability of utilizing low-cost agricultural sources, which are renewable in nature. Moreover, this avenue of research contributes to the prudent recycling of agricultural by productsh, thereby addressing potential environmental hazards, particularly within the realm of solid waste management [10]

Emerging trends within scientific inquiry have spurred the exploration of alternative, economically feasible adsorbents. In a noteworthy example, baobab fruit shells have been harnessed for their adsorptive potential, effectively removing Pb(II) and Cu(II) ions from aqueous solutions [11]. Further innovation has seen the creation of activated carbon derived from baobab fruit shells, successfully utilized for the adsorption of Pb(II) and Cd(II) ions present in synthetic wastewaters [12]. In a similar vein, diverse agricultural residues have been harnessed for activated carbon synthesis. This includes the utilization of date stone [13], rubber wood sawdust [3], bamboo-based materials [2], mango seeds [14], kola nut shells [15], as well as the hulls of coconut and palm tree seeds [16,17]. Each of these unconventional adsorbents exhibits promising potential for addressing heavy metal contamination in diverse contexts.

In the scope of this investigation, baobab pulp activated carbon (BAC) and mango seed activated carbon (MAC) were judiciously employed as potent adsorbents, effectively targeting the removal of Pb(II) from aqueous solutions. This study comprehensively delved into the influence of pivotal process variables, including the initial concentration of metal ions, adsorbent dosage, contact duration, pH, temperature, and the desorption process.

The equilibrium isotherm data, a cornerstone of adsorption analysis, underwent rigorous scrutiny through the application of the Langmuir, Freundlich, and Temkin isotherm models. Concomitantly, diverse adsorption kinetic models were meticulously employed to evaluate the experimental data, encompassing the Pseudo-first order, Pseudo-second order, and Intra-particle diffusion models. The endeavour extended to the exploration of essential thermodynamic parameters, namely free energy (ΔG), enthalpy (ΔH), and entropy (ΔS), which collectively contribute to the comprehensive understanding of the adsorption process.

In tandem with these analytical pursuits, a diverse array of advanced techniques was harnessed. Notably, the Fourier-transform infrared spectrophotometer (FTIR) facilitated the elucidation of surface functional groups, thereby unraveling the intricate composition of BAC and MAC. Furthermore, the microscopic examination of the adsorbents' morphology was facilitated by the Scanning Electron Microscope. A precise quantification of the elemental constituents—carbon, hydrogen, nitrogen, and sulfur—was realized through the employment of a Carbon, Hydrogen, Nitrogen, and Sulfur (CHNS) analyzer, thereby enabling an enhanced understanding of the adsorbents' elemental composition.

The pivotal matter of desorption was accorded thorough investigation. This encompassed a meticulous desorption study conducted employing distilled water, as well as an assortment of acid solutions of varying concentrations. Such a comprehensive approach inherently contributes to a nuanced comprehension of the desorption dynamics of the adsorbents.

2. METHODOLOGY

Baobab pulps and Mango fruit were collected from baobab and Mango trees within the University of Ilorin premises located at about 1km away from the main gate of University of Ilorin, Kwara State Nigeria. Lead (II) nitrate, potassium dichromate and phosphoric acid that were used in this study were of analytical grade and were used without further purification. The impregnating agent used for the chemical activation of baobab pulp was H_3PO_4, apparatus such as; mechanical shaker, magnetic stirrer, pH meter, desiccator, conical flask, thermometer, electric oven with thermostat, analytical weighing balance were also employed in this study.

The baobab pulp and mango seeds were washed thoroughly with deionized water to remove dirt/unwanted parts and dried very well in a shade until constant weight was achieved. The stock solution of 1000 ppm of Pb(II) was prepared by dissolving 1.5980 g in 1000 cm^3 of volumetric flask and made up to mark with deionized water. Working solution was prepared from the stock solution by serial dilutions.

Two major steps were used in the production of activated carbon. These are carbonization and activation (Nsi et al., 2016). The sample materials were carbonized in an inert atmosphere under continuous flow of N_2 in a pyrolyser. A 100 g of the dried raw samples were weighed and charred in a pyrolyser at 500 ^oC. The charred product was allowed to cool down to room temperature and re-weighed. They were ground into workable size ranges with mortar and pestle. The samples at this stage were purified by soaking in 0.5 M Hydrochloric acid solution for 24 hrs, rinsed with deionized water severally until the pH of washed water was neutral. Activation was carried out in a muffle furnace, using 0.1 M orthophosphoric acid (H_3PO_4) as activating agent in the ratio of 1:1 by weight of charcoal/H_3PO_4. A 25 g of each carbonized product was weighed and transferred into 500 ml beaker containing 1.0M solution of orthophosphoric acid. The content of the beaker was mixed thoroughly and heated until paste was formed. A crucible was cleaned and heated to a constant weight. The paste was then transferred into the crucible and this was later placed in the furnace and activated at 500 ^oC for three hours. The activated products were allowed to cool to room temperature, wash with deionized water until the pH of the washed water was neutral and then dried in the oven at 100 ^oC for 24 hours. The activated carbon yield was calculated by applying the formula:

$$X\ (\%) = \frac{m}{m0}\ x\ 100 \quad (1)$$

Where X is char or activated carbon yield (%), m is the char or activated carbon mass (g) and m_o is the raw sample mass (g). Thus, X is an average value of all the effective experiments [10].

2.1 Characterization of Adsorbents

The activated carbon obtained from baobab pulp and mango seed shell were characterized for moisture content [18], bulk density [19], ash content [20], determination of iodine number [14], determination of pH of point of zero charge (pH_{pzc}) [21], volatile matter [14], activated carbon/charcoal yield and pH using standard procedures [21].

The adsorption of Pb(II) ions on BAC and MAC were studied by batch adsorption. The effect of initial adsorbate concentration (range 25 - 500 ppm), adsorbent dose (0.2 - 1.0 g), contact time (5 - 180 min), solution pH (2 - 9) and temperature (30 - 70 ^oC) were examined.

Adsorption parameters were optimized in order to understand the adsorption capacity of the two adsorbents (BAC and MAC).

2.1.1 Effect of initial adsorbate concentration

Different concentrations of 25, 50, 100, 150, 250, 350 and 500 ppm of Pb(II) were prepared by serial dilution from the stock solutions. A 25 ml of each concentration was measured in to 100 ml capacity conical flask containing 0.5 g of each of adsorbent BAC and MAC. The solution was agitated on a thermostat, orbital shaker for period of 5 hr each and was filtered. The un-adsorbed concentration in the filtrate was analysed using AAS. The quantity adsorbed, Q_e was calculated from equation (2). The initial concentration with the highest (optimal concentration) adsorption was used in subsequent experiments. Experiment was conducted in duplicate.

$$Q_e = \frac{C_o - C_e}{M} x\ V \quad (2)$$

Where: Q_e, is the amount of adsorbate ion adsorbed on the adsorbent at equilibrium (mg/g), C_o is the initial concentration of analyte ion in the solution (mg/l), C_e is the equilibrium

concentration of analyte ion in the solution (mg/l), V is the volume of the solution used (ml), M is the mass of activated carbon used (g).

2.1.2 Effect of adsorbent dosage

A 25 ml of the optimal concentration of the adsorbate (Pb^{2+}) was contacted with varying masses (0.2, 0.4, 0.6, 0.8, and 1.0 g) of the adsorbents, BAC and MAC. The resultant mixture was agitated on thermostat, orbital mechanical shaker for 5 hr at 30ºC. The final solution was filtered and the un-adsorbed concentration in the filtrate was analyzed using AAS. The concentration of the adsorbed metal ion was calculated from equation (2). The optimal adsorbent dose was determined and used for subsequent experiments.

2.1.3 Effect of contact time

The effect of contact time on adsorption capacity was studied using the optimal dose of each adsorbent in well labelled 100 ml conical flasks containing 25 ml of the optimal concentration of the adsorbate Pb(II). The resultant mixture was agitated at 30 ºC on a mechanical shaker at different contact time of 5, 10, 20, 40, 60, 90, 120 and 180 min. At the completion of the predetermined contact time, the solution was filtered and the un-adsorbed concentration in the filtrate was analyzed using AAS.

The concentration of the adsorbed metal ion was calculated from equation (2). The optimal contact time for each adsorbate was determined and used for subsequence experiments. The experiment was carried out in duplicate.

2.1.4 Effect of pH

A 25 ml of the optimal concentration of the adsorbate Pb(II) was adjusted to pH of 2, 3, 4, 5, 6, 7, 8 and 9 by adding either 0.1 M NaOH or 0.1 M HCl. These solutions were contacted with the optimal dose of the adsorbents BAC and MAC followed by agitation on a mechanical shaker for the optimal contact time at 30 ºC. The solution was filtered and the un-adsorbed concentration in the filtrate was analyzed using AAS. The concentration of the adsorbed metal ion was calculated from equation (2). The optimal pH for adsorption of each adsorbate was determined and be used for subsequent experiments.

2.1.5 Effect of temperature

A 25 ml of the optimal concentration of the adsorbate Pb(II) was adjusted to the optimal pH of adsorption and contacted with the optimal dose of each adsorbent. The resultant mixture was then shaken on a mechanical shaker for the optimal contact time at different temperatures of 30, 40, 50, 60 and 70 ºC. The solution was filtered and the un-adsorbed concentration in the filtrate was analyzed using AAS. The concentration of the adsorbed metal ion was calculated from equation (2). The optimal temperature for the adsorption process of each adsorbate was determined and used for subsequent experiments.

2.2 Desorption Experiment

“The normal sorption procedure was carried out using 0.5 g of BAC and MAC samples in 25 ml of the optimal concentration of Pb(II) in 100 ml capacity conical flask. The solution was equilibrated for 5 hr each, the solution was filtered and analyzed for Pb(II) using AAS while the residue was used for desorption experiment. A 25 ml of different concentrations of HCl (0.1, 0.2, 0.5 and 1.0 M) and distilled water were added to the residues in different conical flasks and each solution was equilibrated for 5 hr, the solution was filtered. The filtrate was analyzed using AAS for the amount of Pb(II) released back in to the solution. This sorption and desorption processes were repeated on the same sample for three times cycles. The quantity desorbed was calculated using equation (2) above. A graph of the percentage desorbed was plotted against the cycles of desorption process for the different ionic strengths to ascertain the efficiency of BAC and MAC” [11].

2.2.1 Adsorption isotherm

“Adsorption isotherm is the relationship at a given temperature between the amount of substance adsorbed and its concentration in the solution” [22]. “A variety of isotherm equations have been in used, some of which have a strong theoretical base and some being of mere empirical nature. The equilibrium models that were used in this research work include Freundlich, Langmuir, Temkin. These isotherm equations were used to find out the relationship between the equilibrium concentration of the adsorbate in the liquid phase and that in the solid phase” [23].

The distribution of a solute in the effluent between the adsorbent and the liquid phase is commonly described using the Langmuir model. This model is employed to assess the extent of

adsorption of a solute, such as a heavy metal from an aqueous solution or effluent, onto an adsorbent material [22].

$$\frac{C_e}{Q_e} = \frac{1}{bQ_m} + [\frac{Ce}{Q_m}] \quad (3)$$

Where: Q_m is the monolayer adsorption capacity of the adsorbent (mg/g), is the maximum amount adsorbed, C_e is the Langmuir adsorption constant (mg/l**)** related to energy of adsorption which quantitatively reflects the affinity between the adsorbent and adsorbate**,** C_e is the equilibrium concentration of the solute in the bulk solution (mg/l) and q_e is the amount of solute adsorbed per unit weight of adsorbent at equilibrium (mg/g). The plot of C_e/q_e versus C_e was plotted, the slope and the intercept of the curve were $1/Q_m$ and $1/bQ_m$, respectively.

"The adsorption data obtained from the adsorption of Pb(II) was tested for fitness of data against the Langmuir's adsorption isotherms. The favourability of this adsorption process was subjected to the equation of separation factor or equilibrium parameter R_L" [24].

$$R_L = \frac{1}{1+bC_i} \quad (4)$$

Where b is Langmuir equilibrium constant (mg/l), C_i is highest initial metal ion concentration. For a favourable adsorption, ($0 < R_L < 1$), while for an unfavourable adsorption, ($R_L > 1$), and when ($R_L = 0$), the adsorption is irreversible, and for a linear adsorption behaviour (RL = 1) [25].

The Freundlich theory is predicated on the notion that the adsorbent possesses a heterogeneous surface comprised of various categories of assumption sites. It is postulated that adsorption on each distinct class of site adheres to the principles outlined in the Langmuir isotherm theory [26]. The equation representing the Freundlich adsorption isotherm is given by:

$$q_e = K_f C_e^{\frac{1}{n}} \quad (5)$$

The linearized form of Freundlich equation is:

$$logQ_e = logKf + \frac{1}{n} logC_e \quad (6)$$

where C_e and Q_e are the equilibrium concentrations of the adsorbate in the liquid phase and in the solid phase, respectively, and K_f and n are Freundlich coefficients relating to overall adsorption capacity (mg/g) and surface heterogeneity (dimensionless), respectively [27]. Freundlich constant n also explained how favourable adsorption process will be. When the value of 1/n is greater than one, that is, 1/n > 1, it shows that the adsorption process is favourable and when the value of 1/n is less than one, that is, 1/n < 1, it is an indication that the adsorption process is less favourable.

The Temkin isotherm equation postulates that as the coverage layer of adsorbate on the surface of the adsorbent increases, the heat of adsorption (ΔH_{ads}) for all molecules within that layer decreases in a linear fashion with increasing coverage. The Temkin Isotherm model can be delineated by the following equation:

$$Q_e = \frac{RT}{b} L_n k_T + \frac{RT}{b} L_n C_e \quad (7)$$

Where, R is the universal gas constant (0.008314 $kJmol^{-1}.K$); T is the absolute temperature (K); $\frac{1}{b}$ is the Temkin constant related to the heat of adsorption (kJ/mol) which indicate the adsorption potential (intensity) of the adsorbent and k_T (L/g) is the Temkin constant related to adsorption capacity. Plotting q_e versus ln (C_e), this equation results in a straight line of slope $\frac{RT}{b}$and intercept $\frac{RTL_nk_T}{b}$ [28] - [30].

2.3 Adsorption Kinetics Models

"Adsorption kinetic models correlate the adsorbate uptake rate with bulk concentration of the adsorbate. The studies of adsorption equilibrium are important in determining the effectiveness of adsorption; however, it is also necessary to identify the types of adsorption mechanism in each system. In this study, four different models were used to predict the adsorption kinetic of Pb(II) on baobab pulp activated carbon and mango seed shell activated carbon. These are: Pseudo-first-order, Pseudo-second-order, Intra-particle diffusion and Bangham's model" [11], [31].

2.3.1 Pseudo-first-order rate kinetic model

Pseudo-first-order equation given by [32] was employed to determine the rate constant of the adsorption process. The equation for the reaction is:

$$\frac{dQ}{dt} = k(Q_e - Q_t) \quad (8)$$

Where Q_e is the quantity of solute adsorbed at equilibrium per unit mass of adsorbent (mg/g), Q_t

is the amount of adsorbate adsorbed at any given time t, (mg/g) and k is the constant of first order sorption (min^{-1}). To integrate the above equation, the boundary conditions will be set within the range t = 0 to t = t and Q_t= 0 to Q_t = t and simplifying the result of integration the above equation becomes:

$$log\ log\ (Qe - Q_t)\ = log\ log\ Q_e\ - \frac{k}{2{\cdot}303}t \quad (9)$$

The plot of $log\ log\ (Qe - Q_t)$ against t gives the slope and intercept from which k and Q_e can be evaluated.

2.3.2 Pseudo-second-order rate kinetic model

Based on equilibrium adsorption, Pseudo-second-order rate kinetic equation is expressed as:

$$\frac{dQe}{dt} = k_2(Q_e - Q_t)^2 \quad \text{-------} \quad (10)$$

To integrate the above equation, the boundary conditions will be set within the range t = 0 to t = t and Q_t = 0 to Q_t = Q_t and simplifying the result of integration, the above equation becomes:

$$\frac{t}{q_t} = \frac{1}{k_2 Qe^2} + \frac{1}{Qe}t \quad (11)$$

Where k_2 is the rate constant of second order adsorption (g/mg min). The values of k_2 and Qe will be obtained from the plot of $\frac{t}{q_t}$ against t.

2.3.3 Intra-particle diffusion and Bangham's model

In order to investigate the mechanism of Pb(II) adsorption onto activated carbon from baobab and Mango seed shell, intra-particle diffusion-based mechanism was studied.

The model proposed that in case the data fit well in to its equation, then the uptake of the adsorbate, Pb(II) by the adsorbent will varies almost proportionately with the square root of the contact time ($t^{1/2}$). The model equation is given as:

$$q_t = k_{id}\sqrt{t} + C \quad (12)$$

Where, q_t is the amount of adsorbate adsorbed per unit mass of adsorbent (mg/g) at a time t, and k_{id} is the intra-particle diffusion rate constant ($mg/g.min^{-1/2}$). "The rate constant was obtained from the slope of the straight line of q_t against $\sqrt{t}$ and if these lines pass through the origin, then intra-particle diffusion is the rate determining step. When the plots do not pass through the origin, this is indicative of some degree of boundary layer control and this further show that the intra-particle diffusion is not the only rate limiting step, but also other kinetic models may control the rate of adsorption, all of which may be operating simultaneously" [33], [34]. Also, to confirm that adsorption process is controlled by intra-particle diffusion model, the intra-particle diffusion coefficient, D_p, was calculated using the equation below:

$$Dp = \frac{0.03\ x\ r^2}{t_{\frac{1}{2}}} \quad (13)$$

Where Dp is the diffusion coefficient with the unit cm^2/s; $t_{1/2}$ is the time (s) required to complete half of the adsorption and r is the average radius of the adsorbent particle in cm. If the calculated intra-particle diffusion coefficient (Dp) value is in the range of 10^{-11} to 10^{-13} cm^2s^{-1}, then the intra-particle diffusion controls the rate limiting step and, if the calculated film diffusion co-efficient (D_F) value is in the range of 10^{-6} to 10^{-8} $cm^2.s^{-1}$, then the rate limiting step is controlled by film (boundary layer) diffusion. The D_F values are calculated as follows:

$$Df = \frac{(0.23r^2\ \delta Cs\ )}{Cl.t_{\frac{1}{2}}} \quad (14)$$

Where r^2 and $t_{1/2}$ have the same meaning as before, δ is the film thickness (10^{-3} cm), C_s and C_l are the concentrations of adsorbate in solid and liquid phase at time t, respectively [34], [35].

2.4 Thermodynamic Parameters

The thermodynamic parameters of the adsorption process, such as free energy change (ΔG^0), enthalpy change (ΔH) and entropy change (ΔS), give information about spontaneity, heat change and degree of freedom of the adsorbed species respectively, the parameters are also very important in predicting the adsorption mechanism, for characterization and optimization of the process, as well as for equipment and process design.

The idea of adsorption can be fully expressed by examining the following thermodynamic parameters such as free energy (ΔG^0), enthalpy change (ΔH), entropy change (ΔS) and activation energy (E_a).

2.4.1 The Gibb's free energy change, (ΔG^0)

The negative values indicate that the adsorption process is spontaneous at the range of temperature studied. The decrease in the negative value of ∆G with an increase in temperature indicates that adsorption process is more favourable at higher temperatures. Standard free energy (ΔG^0) was calculated from the following equations:

$$k_C = \frac{Q_e}{C_e} \quad (15)$$

$$\Delta G_0 = -RTlnK_C \quad (16)$$

$$\Delta G_0 = \Delta H_0 - T\Delta S_0 \quad (17)$$

Where, T is the temperature (K), R is the gas constant (kJ/mol.K) and K_C (L/g) is the standard thermodynamic equilibrium constant, Q_e is the amount of adsorbate adsorbed per unit mass (mg/g) of adsorbent at equilibrium and C_e is the equilibrium aqueous concentration of adsorbate(mg/L) [36].

2.4.2 Enthalpy change, (Δ H) and entropy change, (ΔS)

These two parameters can be obtained from the equation:

$$\Delta G^\circ = -RTlnK_C \quad (18)$$

$$L_nK_C = -\frac{\Delta H}{RT} + \frac{\Delta S}{R} \quad (19)$$

The value of ΔH and ΔS was obtained from the slope and intercept respectively of the plot $\ln K_C$ versus 1/T. "The positive values ΔH indicate the presence of an energy barrier in the adsorption and endothermic process while the negative ΔH values indicate that the process is exothermic, and a given amount of heat is evolved during the binding of metal ion on the surface of adsorbent" [2]. "The positive value of entropy change (ΔS) indicates strong affinity of adsorbate towards adsorbent and increased in the degree of randomness (disorder) at solid-solution interface during adsorption process" [34].

2.4.3 The Activation Energy of Adsorption, (E_a)

The activation energy (E_a) in adsorption process is defined as the minimum energy required for the adsorbate species to interact with the adsorbent surface. This parameter determines how dependent the adsorption rate is on temperature. The activation energy for the adsorption of Pb(II) onto activated carbon from baobab pulp and mango seed were evaluated using the Arrhenius equation (Chayande et al., 2013)

$$K_C = Ae^{-Ea/RT} \text{ -------} \quad (20)$$

This can be linearized as:

$$LK_c = LnA - \frac{Ea}{RT} \text{ -------} \quad (21)$$

Where, K_c is the concentration equilibrium constant, A is the pre-exponential factor, E_a is the Arrhenius activation energy, which indicates whether adsorption is mainly physical or chemical in nature and also it must be overcome for adsorption to occur. R is the gas constant and T is the absolute temperature in K. E_a and A can be obtained from slope and intercept of a plot of $\ln K_c$ against 1/t which will give a straight line [38].

2.5 Instrumentation

The methods used to characterize the activated carbon includes the following: Fourier Transform Infrared (FTIR), Scanning electron microscope (SEM) and CHNS analyzer.

3. RESULTS AND DISCUSSION

3.1 Carbonization Process

The study investigated the significant impact of the changes in charring temperature and duration on important parameters such as surface area, adsorbent yield, and bulk density. These physicochemical properties serve as indicators of the potential commercial utility of the experimental charred carbon [9]. The physicochemical characteristics, presented in Table 1, offer insights into the suitability of the adsorbent for specific processes [39]. Percentage yield, a key parameter, serves to gauge the efficiency of the carbonization process, with a higher yield being vital for economically viable activated carbon production. The outcomes of percentage yield for char under different conditions are detailed in Table 1. Notably, the peak percentage yield was achieved at a charring temperature of 400°C and a charring time of 150 minutes for both baobab (B) and mango (M). This trend is attributed to the loss of volatile components intensifying with increased temperature and time during carbonization, leading to a reduction in percentage yield [40].

Table 1. Carbonization time and temperature for baobab and mango fruit

Sample code	B_1	B_2	B_3	B_4	M_1	M_2	M_3	M_4
Charring temperature (°C)	400	400	400	500	400	400	400	500
Charring time (mins)	180	210	150	200	180	210	150	200
Yield (%)	21.92	22.40	30.74	20.02	22.14	23.06	28.28	19.64

Key: B = Baobab, M = Mango

For samples labelled BAC and MAC, the most substantial observed percentage yields were 30.74% and 28.28%, respectively, under experimental conditions of 400°C for 150 minutes. This significantly outperformed the yields of 20.02% and 19.64% for samples B and M, respectively, obtained under an experimental condition of 500°C for 200 minutes. The adverse impact of higher carbonization temperatures and longer durations is particularly evident at the elevated experimental temperature of 500°C [41]. One of the key studies investigating the impact of carbonization temperature on seed properties was conducted by [86]. They examined the carbonization of lignocellulosic biomass, including seeds, at different temperatures ranging from 300°C to 900°C. It was found that increasing the carbonization temperature resulted in enhanced carbon content and improved structural stability of the seeds. These changes are attributed to the decomposition and volatilization of low molecular weight compounds, such as cellulose, hemicellulose, and lignin, present in the seeds during carbonization.

Moreover, the carbonization temperature also affects the chemical composition and functional groups present in the resulting carbonized seeds. According to a study by [87], the carbonization temperature influenced the elemental composition, surface area, and pore structure of activated carbons prepared from seeds. The authors found that higher carbonization temperatures led to an increase in carbon and oxygen contents, while nitrogen and sulfur contents decreased. The surface area and pore volume of the activated carbons also increased with increasing carbonization temperature, resulting in improved adsorption properties.

3.2 Physicochemical Characteristics of BAC and MAC

The presence of volatile matter in the prepared BAC and MAC is attributed to residual organic compounds. The obtained volatile matter percentages were 25.60% for BAC and 15.0% for MAC. These values exceed the reported value of 20.9% by [42] but are lower than the value of 26.79% reported by [14] using mango seed. The moisture content of BAC and MAC stands at 8.40% and 7.60%, respectively, slightly lower than the reported value of 9.0% by [43].

Table 2 presents the characteristics of the activated carbon produced from Baobab (BAC) and Mango (MAC) in this study. The ash content reflects the inorganic constituents and was found to be 4.80% for BAC and 2.40% for MAC. These values are higher than the 2.33% reported by [14] using mango seed and align with the 8.2% reported by [43]. Most activated carbon from agricultural sources typically has ash content within the range of 0.2-13.4% [44].

Bulk density and particle size of the adsorbent are vital parameters to consider before applying it in a treatment system. Adsorbent density depends on the starting material and the preparation process [43]. Bulk density measures the amount of solution (adsorbate) the carbon (adsorbent) can hold per unit volume. It plays a crucial role in designing adsorption columns and impacts the overall cost of the adsorption process [45]. BAC and MAC exhibit bulk densities of 0.694 g/cm3 and 0.64 g/cm3, respectively (Table 2). These values are relatively high and comparable to those reported in the literature. For instance, [40] reported bulk densities ranging from 0.6233 to 0.6952 g/cm3 for palm kernel shell pyrolyzed at 1000, 900, and 800°C for 15-45 minutes. Additionally, [46] reported a bulk density of 0.5162 g/cm3 for palm oil shell pyrolyzed at 800°C for 60 minutes. Higher bulk density also contributes to greater mechanical strength [47].

The pH values of BAC and MAC were measured to be 7.73 and 7.58, respectively, slightly exceeding the reported values of 6.3 and 6.8 by [48-50]. Carbon with a pH range of 6-8 is generally suitable for various applications like sugar decolorization and water treatment, as

indicated by [1]. “The pH is influenced not only by the presence of carbon dioxide but also by organic and inorganic solutes present in the water. Changes in water pH are often linked to alterations in other physicochemical parameters” [20].

“The pH at the point of zero charge (pH_{pzc}) of the activated carbon surface is significant since it determines the surface charge under different solution pH conditions. When the solution pH is lower than the pH_{pzc}, the activated carbon surface carries a positive charge, making it capable of adsorbing anions. Conversely, if the solution pH surpasses the pH_{pzc} of the activated carbon, the surface becomes negatively charged, leading to the adsorption of cations” [48]. The pH_{pzc} values for BAC and MAC, depicted in Fig. 1(a & b), were determined to be 7.7 and 8.3, respectively, which exceed the pH_{pzc} value of 6.53 reported by [60] using pomegranate pulp**.** pH point of zero charge (pH_{pzc}) of Baobab Activated Carbon (BAC) (a) and pH point of zero charge (pH_{pzc}) of Mango Activated Carbon (MAC) (b).

3.3 FT-IR Analysis

The FTIR spectra of Baobab activated carbon (BAC) and Mango activated carbon (MAC) were acquired in the range of 4000-400 cm^{-1} before and after the adsorption of Pb(II) ions, with the aim of discerning alterations in the frequencies of functional groups on the adsorbent surface. The spectra were comparatively analyzed to corroborate the successful adsorption of Pb(II) ions.

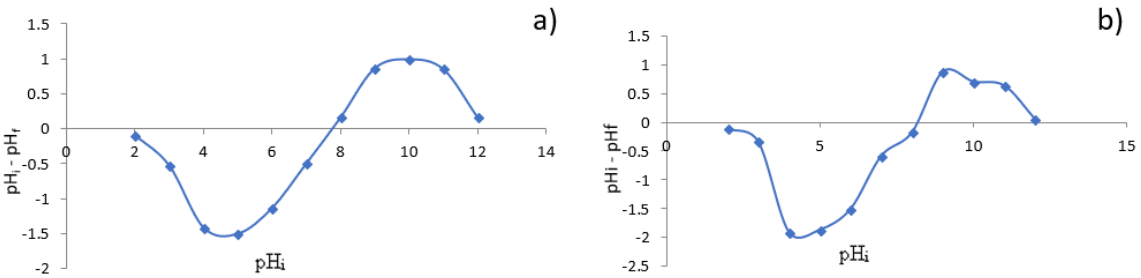

Fig. 1. pH point of zero charge (pH_{pzc}) of Baobab Activated Carbon (BAC) (a), pH point of zero charge (pH_{pzc}) of Mango Activated Carbon (MAC) (b)

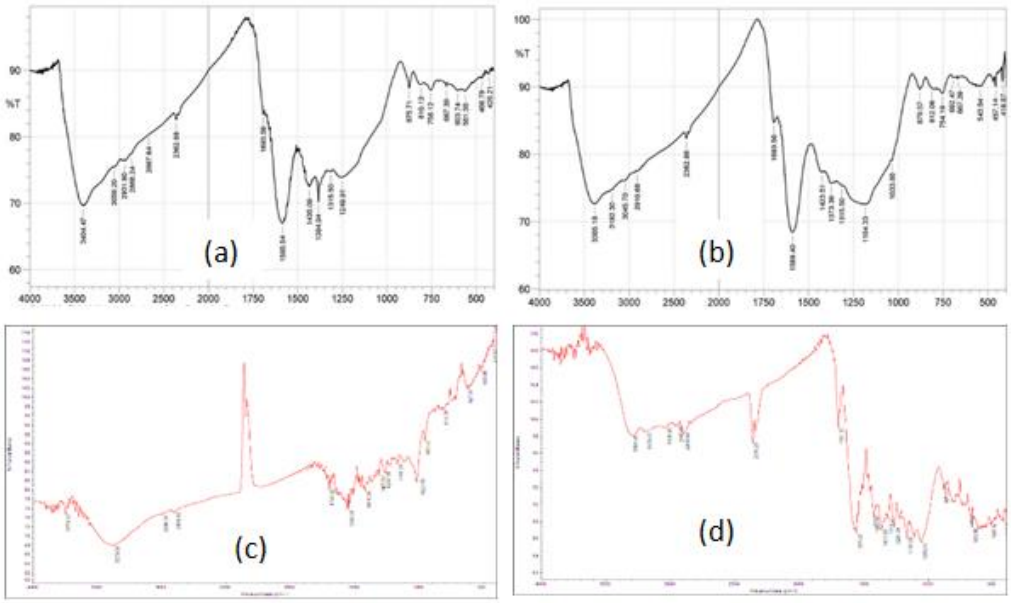

Fig. 2. Fourier transform infrared spectra of unloaded metal ions: BAC (a), MAC (b), and loaded metal ions: BAC (c), MAC (d)

Table 2. Physicochemical Characteristics of BAC and MAC

Parameters	BAC	MAC
pH	7.73	7.53
pH_{pzc}	7.74	8.33
Moisture (%)	8.40	7.60
Volatile matter (%)	25.60	15.0
Ash content (%)	4.80	2.40
Bulk density (gcm^{-3})	0.69	0.64
Surface area (m_2/g)	355.357	360.526

The FTIR spectra of BAC and MAC prior to adsorption are depicted in Fig. 2(a & b). The observed peaks at 3404.47 cm^{-1} (BAC) and 3385.18 cm^{-1} (MAC) were attributed to the O-H stretching vibrations of strongly hydrogen-bonded carboxylic acid (COOH) moieties [51]. Concurrently, the peaks at 2931.90 cm^{-1} (BAC) and 2910.68 cm^{-1} (MAC) were ascribed to the C-H stretching vibrations of CH, CH_2, and CH_3 groups [21]. A prominent absorption band at 1249.91 cm^{-1} (BAC) and 1184.33 cm^{-1} (MAC) indicated C-O stretching vibrations, in accordance with previous research [37]. Furthermore, the presence of a carbonyl group was discerned through the C=O stretching vibration, observed at 1693.56 cm^{-1} for both BAC and MAC. The bending vibrations of CH_3 were manifest in the peaks at 1384.94 cm^{-1} (BAC) and 1373.36 cm^{-1} (MAC), while the CH_2 bending vibrations were indicated by the peaks at 1435.09 cm^{-1} (BAC) and 1423.51 cm^{-1} (MAC). The intense absorption bands observed at 1585.54 cm^{-1} (BAC) and 1589.40 cm^{-1} (MAC) were attributed to the conjugated C=C stretching vibrations, as reported by [37]. Additionally, the bending modes of aromatic compounds were inferred from the peaks around 875.71 cm^{-1} and 810.13 cm^{-1} (BAC), as well as 879.57 cm^{-1} and 812.06 cm^{-1} (MAC), in agreement with previous findings [52].

Upon post-adsorption analysis, as depicted in Fig. 2(c & d), discernible shifts in certain peaks were observed, indicating alterations in the spectra. Notably, the adsorption peaks corresponding to the bonded –OH groups experienced a shift from their initial positions at 3404.47 cm^{-1} and 3385.18 cm^{-1} to 3300.26 cm^{-1} and 3373.09 cm^{-1} for BAC and MAC, respectively. This observation suggested a reduction in hydroxyl polymerization within the biomass, attributed to the presence of metal ions such as Cu (II), Cd (II), Pb (II), and Cr (VI) [53], [54]. This phenomenon alluded to the binding of metal ions to hydroxyl groups, implying a chemical interaction between the metal ions and the hydroxyl groups on the biomass surface.

Furthermore, the initial carbonyl peaks observed at 1693.56 cm^{-1} for both unloaded BAC and MAC exhibited shifts to 1701.32 cm^{-1} and 1704.49 cm^{-1}, respectively, after adsorption. This shift in the wave number of the characteristic C=O group peak from carboxylic acid signified the presence of interactions between carbonyl functional groups and the metal ions. Such a change pointed to the transformation of free carbonyl groups into carboxylate groups (COO-), indicative of reactions between the metal ions and the carbonyl groups present on the adsorbent [26], [55]. “Evidently, the shifts indicated the participation of –OH, –CH, and C=O groups in the adsorption of metal ions, hinting at the likelihood of an ion exchange mechanism at play in the interaction between the biomass and the metal ions” [55].

In addition, the FTIR spectra of both BAC and MAC following metal ion loading displayed distinctive bands within the range of 600-450 cm^{-1}, affirming the presence of Cd-O, Cu-O, Pb-O, and Cr-O stretching modes [48], [56]. These spectral features underscored the existence of chemical interactions between the biomass and the various metal ions. Analogous findings were reported in previous studies focusing on the biosorption of Pb (II), Cd (II), and Cu (II) onto Botrytis cinerea fungal biomass [57], as well as the biosorption of Pb (II) and Cd (II) from aqueous solutions using macro-fungus (*Lactarius scrobiculatus*) biomass [58].

3.4 SEM Morphology Analysis

The examination of the surface morphology of both activated carbon samples, before and after the adsorption process, was conducted using a Teneo LV scanning electron microscope (LVSEM). The process of phosphoric acid activation led to an enhancement in pore development within the activated carbon. This

was achieved as the activation with phosphoric acid caused swelling of the Baobab activated carbon (BAC) and Mango activated carbon (MAC), leading to the expansion of their surface structures. The introduction of activating reagents, such as H_3PO_4, during carbonization facilitated the opening of these pores, which were formed by the subsequent evaporation of the activating agents [60].

The micrographs depicted in Fig. 3(a & c) illustrate the surface structures of MAC and BAC prior to the adsorption process. These images unveiled the presence of irregularly shaped pores characterized by cracks, grooves, and crevices. This intricate porous nature serves to enhance the adsorption capacity for metal ions. It's worth noting that these pores were more abundant in the case of MAC, whereas BAC exhibited wider pore dimensions.

Fig. 3(b & d) on the other hand, present the micrographs of MAC and BAC after the adsorption of Pb(II) ions. These images showcase surfaces with fewer pores, as many of these pores became occupied by the adsorbed metal ions. The micrographs reveal a diminished number of unoccupied adsorption sites, particularly evident in the micrograph of MAC. This observation underscores the effective occupation of these sites by the adsorbed Pb(II) ions. Similar observations were made by [88] on date seeds powder for Ni^{2+} adsorption.

3.5 CHN Analysis

In this study, the result of CHN (Table 3), shows a high percentage of carbon content compared to activated carbon from another adsorbent. BAC contains 70.04 % C, 3.06 % H and 0.67 % N while MAC had 71.44 % C, 2.89 % H and 0.64 % N, the results achieved in this study were observed to be higher than the values obtained by [14] for MGA (52.31 % C, 3.38 % H and 1.02 % N), [60] for ASAC (63.76 % C, 2.54 % H and 0.81 % N) and lower than the values obtained by [59] for Pulp AC, Peel AC and GSPAC.

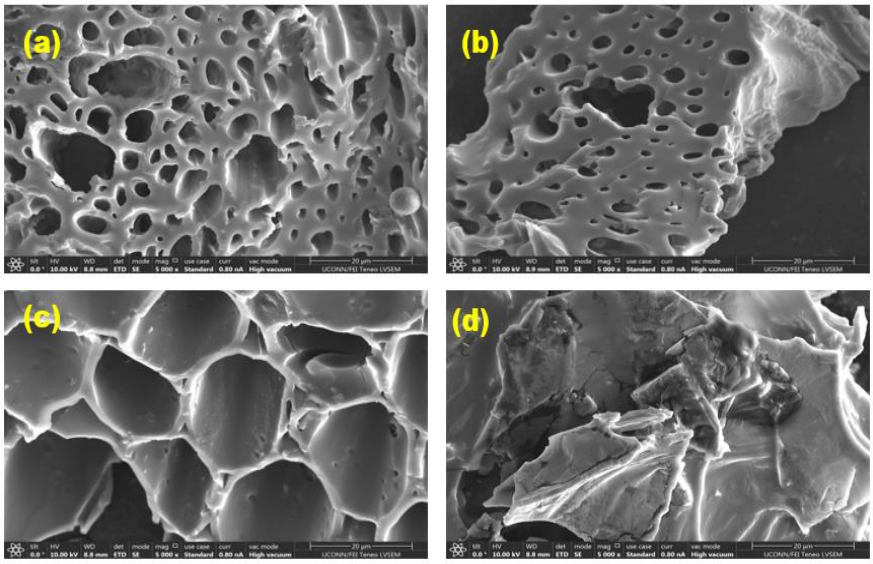

Fig. 3. SEM micrographs of MAC before adsorption (a), MAC after adsorption of Pb(II) (b), BAC before adsorption (c), BAC after adsorption of Pb(II) (d)

Table 3. Comparison of CHN values of activated carbon from different adsorbents

Adsorbent	C	H	N
Pulp AC	74.30	2.77	1.55
Peel AC	72.52	2.75	0.97
MGA	52.31	3.38	1.02
ASAC	63.76	2.54	0.81
GSPAC	75.80	2.95	1.53
BAC	70.04	3.06	0.67

From these results, it shows that CHN values from BAC and MAC were quite encouraging due to the relatively high carbon content. The CHN values obtained from this study were however in the range of values for most agricultural materials as reported by [60]. (41.23-84.50% C, 4.63-6.26% H and 0.7-4.10% N). Similar observations were also made by [89] on walnut shells as an adsorbent for the removal of heavy metals from aqueous solutions. It was found that the activated carbon had high carbon content and low hydrogen and nitrogen content. This information is important for assessing the adsorption capacity and selectivity of the seeds adsorbent towards heavy metals.

3.6 The effect of Process Variables

3.6.1 Initial concentration on adsorption

In Fig. 4a, the graph displays the connection between equilibrium adsorption capacity (q_e) and initial metal ion concentration (C_0). As metal ion loading increases from 25 mg/l to 500 mg/l, both BAC and MAC exhibit a substantial increase in adsorption capacity: BAC rises from 1.1 mg/g to 18.7 mg/g, and MAC from 1.1 mg/g to 16.0 mg/g. This rise is attributed to higher metal ion presence, effectively countering mass transfer limitations and capitalizing on available adsorption sites. This outcome propels an augmented metal uptake, generating a steep rise in the curve representing adsorption capacity against initial concentration.

Furthermore, higher adsorbate loading concentrations lead to increased competition among adsorbate molecules for the limited binding sites on the adsorbent surface. This competition contributes to an enhanced removal of metal ions, as observed in prior studies [5].

The presence of a high concentration of adsorbate molecules in the solution intensified the interaction between the adsorbent and adsorbate. This phenomenon aligns with a similar trend where increased adsorption is directly proportional to higher adsorbate concentrations [61-62]. As the adsorption process advances, the available adsorption sites decrease, leading the curve to converge towards the concentration axis. This behaviour is a result of the diminishing value of q_e as adsorption proceeds.

The equilibrium adsorption capacity demonstrates an increasing trend with rising initial metal ion concentrations. This is attributed to the larger driving force for mass transfer at higher concentrations, resulting in a higher equilibrium uptake. However, a contrasting pattern is observed for the removal percentage of Pb(II) ions, as illustrated in Fig. 7b. Specifically, when the initial concentrations are elevated from 25 mg/l to 500 mg/l, the percentage of Pb(II) ions removed decreases. This behaviour is explained by considering the interplay between the initial number of metal ions in the solution and the available active sites on the adsorbent surface. At lower concentrations, the ratio of initial metal ions to active sites is low [5]. As the initial concentration rises, more metal ions are present in the solution, while the amount of adsorbent remains constant. Consequently, the ratio between metal ions and vacant adsorption sites on the adsorbent becomes larger, leading to a reduction in the removal percentage [5]. Furthermore, the initial adsorption concentration also plays a crucial role in the equilibrium adsorption capacity of the adsorbent material. In a study by [90], they investigated the adsorption of heavy metal ions onto a magnetic graphene oxide-based nanocomposite. The researchers studied the impact of initial adsorption concentration on the adsorption capacity of the nanocomposite. They observed that increasing the initial concentration of the heavy metal ions resulted in a higher equilibrium adsorption capacity of the nanocomposite. This finding highlights the importance of considering the initial adsorption concentration when designing adsorption processes and determining the maximum adsorption capacity of adsorbent materials.

Moreover, the initial adsorption concentration also affects other parameters, such as the adsorption isotherm and the adsorption kinetics. In a study by [91], they investigated the adsorption of dyes onto activated carbon, focusing on the effect of initial adsorption concentration on the adsorption isotherm and kinetics.

3.6.2 Adsorbent Dosage

The rise in the percentage of metal ion removal, from 61.52% to 97.60% for BAC and 55.45% to 95.34% for MAC, corresponding to an increase in adsorbent dosage from 0.2 to 1.0 g (as depicted in Fig. 5(b), is attributable to the augmented surface area that encompasses a greater number of active binding sites [63], [64]. Simultaneously, a decrease in adsorption capacity from 38.4 mg/g to 12.2 mg/g for BAC and 34.7 mg/g to 11.9 mg/g for MAC was

observed as adsorbent dosage increased. This contrary trend is evident in the reduction of the adsorbed metal ions per unit mass of adsorbent (q_e), as presented in Fig. 5(a). The decrease in q_e with higher adsorbent dosage could be attributed to the formation of overlapping adsorbent layers, which restricts access to the active sites, thereby impeding adsorption. This phenomenon aligns with the findings of other researchers [15], [65] who observed similar outcome.

3.6.3 Effect of contact time

Fig. 6(a & b) depict the temporal evolution of adsorption efficiency. Over the duration of 5 to 120 minutes, there was a progressive increase in both the quantity and percentage of adsorption. For Baobab activated carbon (BAC), the uptake rose from 43.27% to 74.43% (10.82 mg/g to 18.61 mg/g), and for Mango activated carbon (MAC), it increased from 30.38% to 64.08% (7.59 mg/g to 16.02 mg/g). This trend persisted until an equilibrium point was reached at around 90 minutes for MAC and 120 minutes for BAC. Subsequently, further increments in adsorption were negligible.

The initial rapid adsorption rate observed within the first 10 minutes may be attributed to the availability of unoccupied active surfaces on the adsorbents for Pb(II) species in the solution. Following this, a moderate rate of removal ensued (10-60 minutes for BAC and 10-90 minutes for MAC). The subsequent deceleration in adsorption (60-180 minutes for BAC and 90-180 minutes for MAC) can be ascribed to electrostatic hindrance due to the presence of previously adsorbed species, coupled with the sluggish pore diffusion of ions and limited access to remaining active sites [66]. The saturation curve exhibits a steep ascent in its early stages, signifying the existence of numerous vacant sites for adsorption initiation. As the curve reaches a plateau, it signifies that the adsorbent is saturated at this level [39], [67-68].

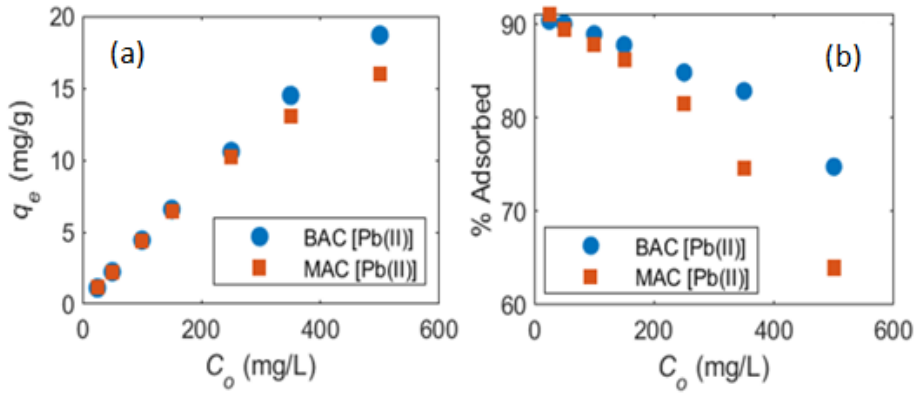

Fig. 4. Effect of Initial Concentration on Amount of Metal adsorbed (a), effect of Initial Concentration on Percentage of Metal Adsorbed (b)

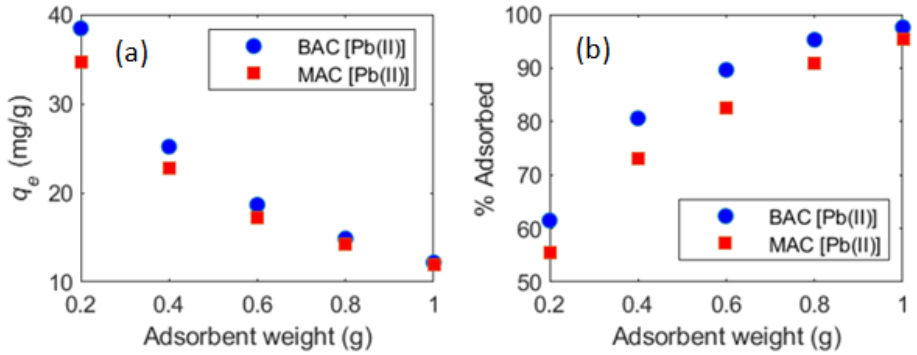

Fig. 5. Effect of adsorbent weight on amount of metal adsorbed (a), effect of adsorbent weight on percentage of metal adsorbed (b)

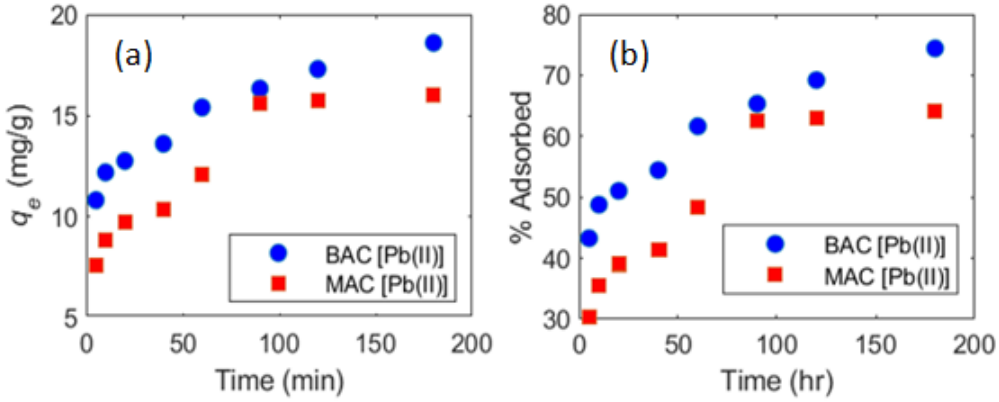

Fig. 6. Effect of contact time on amount of metal adsorbed (a), effect of contact time on percentage of metal adsorbed (b)

3.6.4 Effect of pH

The pH of a solution plays a pivotal role in influencing biomass surface characteristics, metal ion speciation in aqueous environments, and the ionization of surface functional groups [2]. Investigation into the adsorption behaviour of Pb(II) on BAC and MAC was carried out across varying pH levels, with the corresponding data presented in Fig. 7(a and b).

The findings reveal an enhancement in metal ion uptake capacity for both BAC and MAC within the pH range of 2 to 7. Specifically, the uptake capacity for BAC increased from 12.89 mg/l to 25.00 mg/l, while for MAC, it ranged from 11.22 mg/l to 24.21 mg/l. It's important to note that the solubility of most metals decreases at pH levels above 7, potentially leading to precipitation. Therefore, the values of qe attained at pH 8 and 9 may stem from a combined effect of both adsorption and precipitation. Moreover, the concept of pH at the point of zero charge (pH_{pzc}) may elucidate the decrease observed beyond pH 7 for BAC (pH_{pzc} of 8.2) and MAC (pH_{pzc} of 7.8). Beyond the pH_{pzc}, the surface of the adsorbent becomes negatively charged, promoting the enhanced adsorption of positively charged Pb(II) ions through electrostatic attraction [46]. One study that highlights the effect of pH on metal ions adsorption is conducted by [92]. They investigated the adsorption of heavy metal ions (such as cadmium, copper, and nickel) onto activated carbon. The authors found that the pH of the solution significantly influenced the adsorption capacity of the activated carbon. They observed that the adsorption of metal ions increased at lower pH values due to the increasing positive charge on the adsorbent surface, which enhanced the electrostatic attraction between the adsorbent and the metal ions.

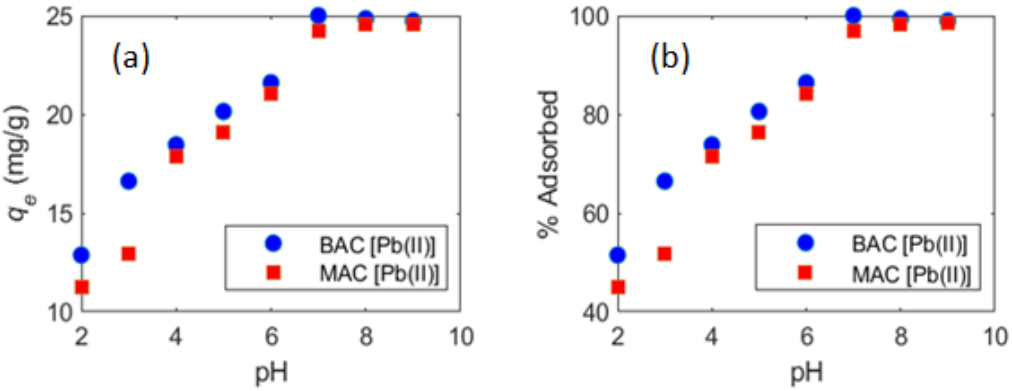

Fig. 7. Effect of pH on amount of metal adsorbed (a), effect of pH on percentage of metal adsorbed (b)

Another study by [93] focused on the adsorption of arsenic ions onto iron-based adsorbents. The authors examined the effect of pH on the adsorption efficiency and found that the adsorption capacity increased with increasing pH for both acidic and neutral pH values. This was attributed to the deprotonation of the active sites on the adsorbent surface, resulting in more favourable adsorption of arsenic ions.

3.6.5 Effect of temperature

The adsorption behaviour of Pb(II) onto BAC and MAC was investigated across a range of temperatures (30, 40, 50, 60, and 70°C), using an initial lead concentration of 500 mg/l and a constant adsorbent dose of 0.2 g. As depicted in Fig. 8(b), the percentage of adsorbed Pb(II) ions exhibited an upward trend, increasing from 60.29% to 88.84% for BAC and from 54.38% to 86.57% for MAC, with temperature elevation from 30 to 70°C.

This augmentation in adsorption efficiency at higher temperatures can be attributed to several factors. Firstly, the increase in chemical interaction between adsorbate and adsorbent may play a significant role, possibly leading to the formation of new binding sites. Furthermore, the rise in temperature could accelerate the intra-particle diffusion of metal ions into the adsorbent pores, effectively enhancing the adsorption process [69]. The kinetic activity of adsorbate molecules also elevates with temperature, promoting greater mobility. Additionally, the higher temperature might cause the internal structure of the adsorbents to swell, allowing larger adsorbates to penetrate deeper into the structure [52], [70].

Fig. 8(a) demonstrates a gradual increase in adsorption capacity, ranging from 37.70 mg/g to 55.53 mg/g for BAC and 33.99 mg/g to 54.11 mg/g for MAC, as the temperature rises from 30 to 70°C. This observed rise in adsorbed metal ion quantities with increasing temperature could be attributed to the involvement of not just physical adsorption, but also chemical adsorption and, in some cases, bond rupture between the adsorbent and adsorbate [71]. These findings corroborate prior research as reported by [5].

3.7 Isotherm Studies

3.7.1 Adsorption Isotherm

The analysis presented in Table 4 reveals that while all three models exhibit good fit with R^2 values exceeding 0.9. The Langmuir isotherm model outperforms the others, yielding regression coefficients of 0.9977 for BAC and 0.9984 for MAC. The Langmuir model assumes uniform energy of adsorption on the surface, without lateral migration of the adsorbate [72].

As depicted in Table 4, the Langmuir model (R^2 = 0.9977 for BAC and R^2 = 0.9984 for MAC) provides the best fit to the experimental equilibrium adsorption data, followed by the Freundlich model (R^2 = 0.9817 for BAC and R^2 = 0.9713 for MAC), and the Temkin model (R^2 = 0.946 for BAC and R^2= 0.968 for MAC), as inferred from the R^2 values obtained. The maximum monolayer adsorption capacities (q_m) are determined to be 27.03 mg/g for BAC and 19.46 mg/g for MAC.

Table 5 provides a comparative assessment of the Langmuir maximum monolayer adsorption capacity for Pb(II) ions using BAC and MAC in this study, alongside other reported adsorbents by different researchers. The equilibrium constant (KL) values are 0.018 for BAC and 0.025 for MAC.

In relation to the separation factor R_L, the values being less than one and greater than zero indicate the favourable adsorption of Pb(II) ions onto BAC and MAC [73]. The Freundlich constant K_F signifies the sorption capacity of the sorbent, with values of 0.709 for BAC and 0.838 for MAC. The value of n, which reflects deviation from linearity, is above unity, suggesting favourable adsorption.

The Temkin constants K_T and B are found to be 0.339 and 0.399 for BAC, and 4.555 and 3.552 for MAC, respectively. The low values of the Temkin constants suggest a weak interaction between the adsorbate and adsorbent, indicative of an ion-exchange mechanism or physical interaction between Pb(II) and adsorbent surfaces [28].

From these data, the Langmuir, Freundlich and Temkin Isotherms for the adsorption process were obtained and are shown in Fig. 9(a, b & c) respectively for BAC and Fig. 9(c, d & e) respectively for MAC.

3.8 Adsorption Kinetics Study

The slope and intercept plot of log (q_e – q_t) against t (Fig. 10a) were obtained to calculate the first order rate constant k_1 and q_e shown in Table 6, which shows an agreement of

experimental data with pseudo first order kinetic model with correlation coefficient R^2, 0.9037 and 0.9297 for BAC and MAC. However, the q_e values of 11.184 and 18.776 mg/g for BAC and MAC respectively were not in agreement with their experimental q_e value of 18.693 and 16.024 mg/g respectively. This shows that pseudo first order does not describe the experimental process. The pseudo second order constant k_2 and q_e were obtained from the slope and intercept of the plot t/q_t versus t (Fig. 10b), which shows a good agreement of experimental data with regression coefficient of 0.9935 and 0.9848 for BAC and MAC. It is important to note that the calculated q_e values of 19.011 and 17.241 mg/g for the adsorption of Pb (II) ions onto BAC and MAC respectively are in close agreement with their experimental q_e values of 18.693 and 16.024 mg/g. Therefore, the pseudo second order model is satisfactorily applicable to the adsorption of Pb(II) ions on the BAC and MAC. Similar result was also obtained by [33], [80].

"The kinetic data were further subjected to intra-particle diffusion model. Fig.10c shows the dependence of the amount of adsorbate uptake at time t (q_t) on the square root of time ($t^{1/2}$) to investigate the fitness of intra-particle diffusion mechanism" [22]. For intra-particle diffusion model to be the sole rate-determining step, [10] pointed out that "it is essential for the plot of q_t against $t^{1/2}$ to pass through the origin but this was not attained in this study. In this present study the plot did not pass through the origin". "This shows that although intra-particle diffusion was involved in the adsorption process as seen from the correlation coefficient, R^2, values (0.9859 and 0.9275) for BAC and MAC respectively. It was not the sole rate-controlling step. The calculated intra-particle diffusion coefficient, D_P, for the adsorption of Pb(II) ions on BAC and MAC was in the range 6.55×10^{-7} $cm^2.s^{-1}$ for both adsorbents. D_P values in the range of 10^{-11} to 10^{-13} $cm^2.s^{-1}$ suggest that intra-particle diffusion is the rate limiting step" [81]. However, the calculated values are greater than 10^{-11} $cm^2.s^{-1}$. This reveals that intra-particle diffusion is not the rate-limiting step for Pb(II) adsorption on BAC and MAC.

Table 4. The Isotherm Parameter for Pb(II) Adsorption on BAC and MAC

Isotherm model	Parameter	BAC	MAC
Langmuir Isotherm	K_L ($1.mg^{-1}$)	0.018	0.025
	qm (mg/g)	27.027	19.455
	R_L	0.100	0.075
	R^2	0.9977	0.9984
Fruendlich Isotherm	K_F (mg/g)	0.709	0.838
	n	1.386	1.630
	R^2	0.9817	0.9713
	K_T	0.339	0.399
Temkin Isotherm	B (kj/mol)	4.555	3.552
	R^2	0.946	0.968

Table 5. Comparison of maximum adsorption capacity of different adsorbents for the adsorption of Pb(II)

Adsorbents	Adsorbent Capacity q_m (mg/g)	Reference
Bamboo dust	2.151	[22]
Powder activated carbon	20.7	[75]
coconut	4.38	[16]
seed hull of palm tree	3.77	[16]
Cocoa shells	6.2	[76]
Cocoa shell activated carbon	21.88	[36]
Lichen	12.3	[77]
Coir (Coco nucifera)	18.9	[78]
Fly ash	15.08	[79]
Caulerpa lentillifera	28.7	[20]
Waste baker yeast in ethanol	17.49	[59]
Baobab pulp activated carbon (BAC)	27.03	This work
Mango seed activated carbon (MAC	19.46	This work

Table 6. The Kinetic Parameters for Pb(II) Adsorption on BAC and MAC

Kinetic Models	Parameters	BAC	MAC
Pseudo-first order	K_1 (min^{-1})	-0.023	-0.042
	$q_{e,\ cal}$ (mg/g)	11.184	18.776
	$q_{e,\ exp}$ (mg/g)	18.693	16.024
	R^2	0.9037	0.9297
Pseudo-second order	K_2	0.005	0.004
	$q_{e,\ cal}$ (mg/g)	19.011	17.241
	$q_{e,\ exp}$ (mg/g)	18.693	16.024
	R^2	0.9935	0.9848
Weber and Morris	K_{id} ($mg.g^{-1}.min^{-0.5}$)	0.688	0.833
	R^2	0.9859	0.9275
Elovich	α ($mg.g^{-1}.min^{-1}$)	0.012	0.331
	β ($mg.g^{-1}.min^{-1}$)	0.474	0.390
	R^2	0.9517	0.8991

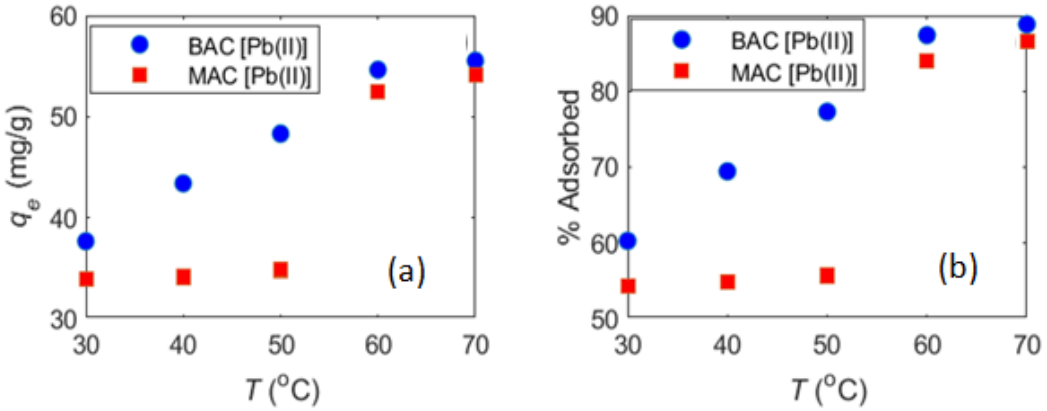

Fig. 8. Effect of temperature on amount of metal adsorbed (a), effect of temperature on percentage of metal adsorbed (b)

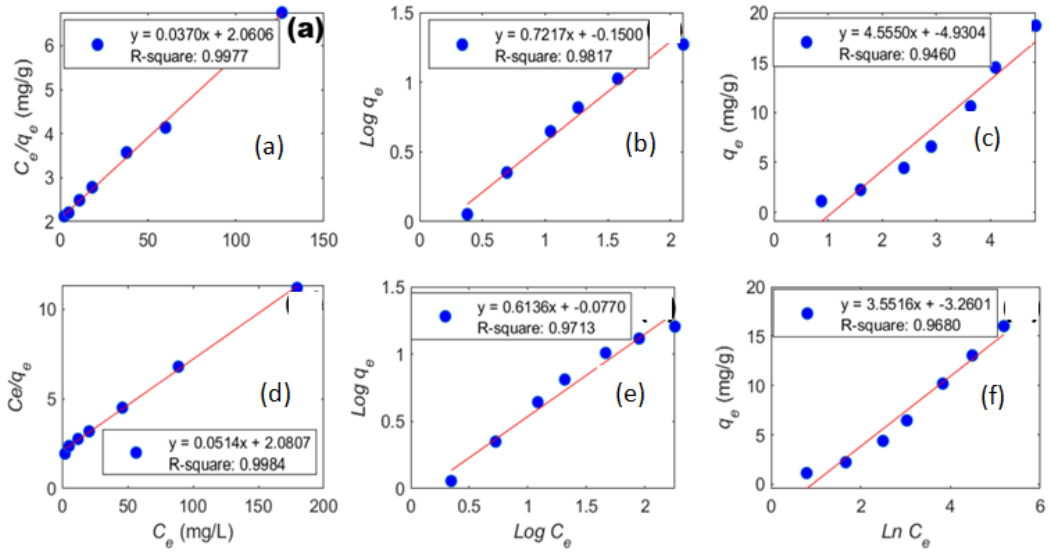

Fig. 9. Langmuir, Freundlich and Temkin isotherms for Pb(II) adsorption on: BAC (a,b,c) respectively and MAC (d,e,f) respectively

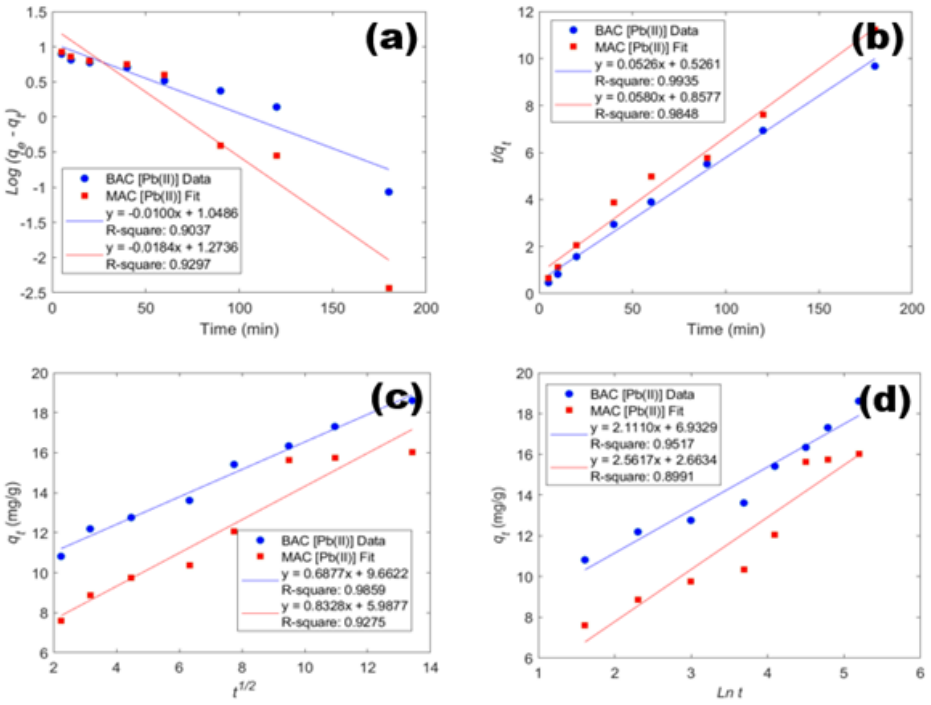

Fig. 10. Pseudo first order plot for Pb(II) adsorption on BAC and MAC (a), pseudo second order plot for Pb(II) Adsorption on BAC and MAC (b), Weber and Morris Plot for Pb(II) Adsorption on BAC and MAC (c), Elovich Plot for Pb(II) Adsorption on BAC and MAC (d)

From Table 7, the calculated film diffusion coefficient (D_F) was found to be in the order of 10^{-8} $cm^2.s^{-1}$ for the adsorption Pb(II) on BAC and MAC. The D_F value in the range of 10^{-6} to 10^{-8} $cm^2.s^{-1}$ shows that the rate-limiting step is governed by film (boundary layer) diffusion [82]. Therefore, the rate of adsorption of Pb(II) on BAC and MAC is governed by film diffusion. The Elovich constant α and β were calculated from the slope and intercept of the plot of q_t versus lnt (Fig. 10d). The R^2 values for Pb(II) on BAC and MAC are 0.9517 and 0.8991 respectively. The small values of β obtained in most cases are in reasonable agreement as reported by [53].

3.9 Thermodynamic Characterization of Batch Adsorption Studies

"The values of ΔH and ΔS (Table 8) for the adsorption of Pb(II) ions on BAC and MAC were calculated from the slope and intercept of the plot of lnKC versus T^{-1} as shown in Fig. 11. The negative values of ΔG from Table 8 increases as temperature increases, which indicates feasibility and spontaneous nature of the adsorption process" [19]. "The positive value of ΔH indicates that the adsorption process is endothermic and higher temperature favours adsorption. The positive value of ΔS reflected that there is good affinity between adsorbent and adsorbate and increased randomness during the adsorption process" [15]. "It also shows that the freedom of metal ions is not too restricted in the biomass confirming a physical adsorption, which is further confirmed by the relatively low values of ΔG" [28]. The ΔG values at all temperature showed that the sorption process was physisorption because the values are lower than (-20 kjmol-1) [83].The activation energy E_a, for BAC and MAC were 0.749 and 0.744 KJ/mol respectively. Therefore, the adsorption process is physisorption since E_a < 42 KJ/mol [72-74].

Table 7. Intra-particle and Film Diffusion Constants for Pb(II) Adsorption on BAC and MAC

Constants	Values	
	BAC	MAC
D_P ($cm^2.s^{-1}$)	6.55×10^{-7}	6.55×10^{-7}
D_F ($cm^2.s^{-1}$)	7.70×10^{-8}	4.47×10^{-8}

3.10 Desorption and Regeneration Studies

The reuse of loaded BAC and MAC adsorbents was examined using adsorption/desorption experiment. Fig. 12a and b, shows the percentage of Pb (II) ion s desorbed in each cycle. The results reveal that in three cycles, the recovery of Pb (II) ion decreases from 91.65 to 28.46 % for BAC and 82.93 to 30.87 % after three regeneration cycles. The result is agreement with what was reported by [84]. The highest Pb (II) ion recovery from BAC-91.65 % and MAC-82.93 % were observed in 0.5 M HCl. The results obtained using distilled water as desorbing agent was very low on both adsorbents (less than 6 %). The adsorption-desorption process was stopped at third cycle to avoid the mass loss of adsorbent dosage. The desorption of Pb (II) ions was reduced from one cycle to another and it may be attributed to the efficiency of functional groups present on the adsorbents being reduced by the acid (HCl) and/or complexation of lead by chloride [85]. From Fig. 12a and b, it reveals that the two adsorbents can be recyclable.

Table 8. Thermodynamic parameters calculated for the adsorption of Pb(II) ions onto BAC and MAC

Adsorbent	T (K)	ΔG (KJmol^{-1})	ΔS (Jmol-1K^{-1})	ΔH (KJmol^{-1})
BAC	303	-2.24		
	313	-2.34		
	323	-2.44	9.86	0.75
	333	-2.53		
	343	-2.63		
MAC	303	-1.03		
	313	-1.08		
	323	-1.14	5.84	0.74
	333	-1.20		
	343	-1.26		

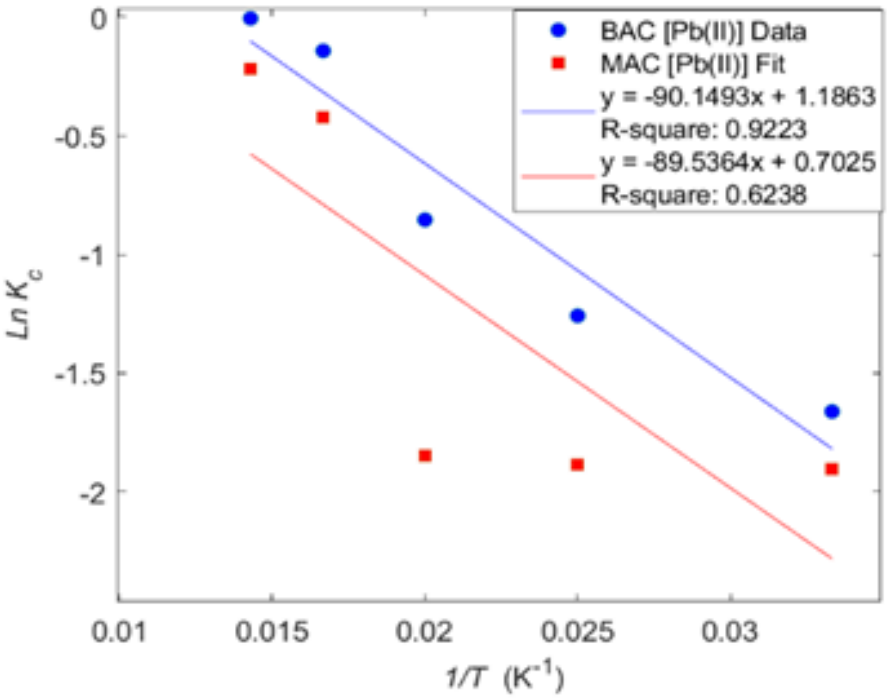

Fig. 11. Plot of lnK$_c$ versus 1/T for sorption of Pb(II) ions on BAC and MAC

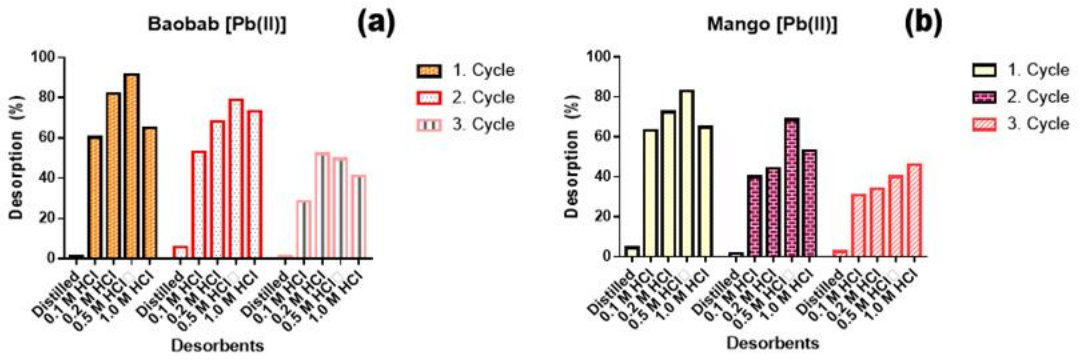

Fig. 12. BAC Pb(II) percentage desorption variation during adsorption-desorption cycles (a), MAC Pb(II) percentage desorption variation during adsorption-desorption cycles (b)

4. CONCLUSION

This study evaluated the activated carbon BAC and MAC made from Baobab pulp (Adansonia digitata) and mango seed as an effective adsorbent for the removal of Pb(II) ions from aqueous solutions. Activation of the raw materials with orthophosphoric acid (H_3PO_4) led to carbons with high adsorption capacities.

The adsorption capacities of BAC and MAC were 18.69 and 16.02 mg/g at 500 mg/L for Pb (II). Adsorption increased with increase in temperature and pH up to a maximum pH value of 7, beyond which the metal ions were precipitated out of their solution as their hydroxides. Adsorption equilibrium was attained at contact time of 90 min. Adsorption capacity q_e, decreases with increase in adsorbent dose (0.2-1.0 g).

The Langmuir adsorption isotherm was found to fit better than other isotherm models by its high correlation coefficient R^2, (> 0.99). All the process was best fitted by pseudo-second order model suggesting that chemisorption process could be the rate-determining step in the adsorption process. Thermodynamic study revealed that the adsorption process was spontaneous, endothermic and increasing randomness of the solid solution interface. The activation energy E_a of the adsorption process was high (< 42 KJ/mol), which indicate physisorption process.

The desorption of about 91.65 % and 82.93 % of the adsorbed Pb (II) ions from BAC and MAC was achieved using 0.5 M HCl. The results demonstrated that activated carbon prepared from baobab pulp and mango seed has the potential to be employed as low-cost adsorbents for both adsorption and desorption of Pb (II).

COMPETING INTERESTS

Authors have declared that no competing interests exist.

REFERENCES

1. Babarinde JOA, Babalola NA. Adesola Babarinde JO. Babalola, Sanni RA. Biosorption of lead ions from aqueous solution by maize leaf Biophysical Chemistry View project Treatment of effluents using adsorption and coagulation/flocculation methods View project Biosorption of lead ions from aqueous solution by maize leaf; 2006. [Online].
Available:
http://www.academicjournals.org/IJPS
2. Ahmad AA, Hameed BH, Aziz N, Adsorption of direct dye on palm ash: Kinetic and equilibrium modeling, J Hazard Mater. 2007;141(1):70-76.
DOI: 10.1016/j.jhazmat.2006.06.094
3. Li S, Han K, Li J, Li M, Lu C, Preparation and characterization of super activated carbon produced from gulfweed by KOH activation, Microporous and Mesoporous Materials. 2017;243:291-300.
DOI: 10.1016/j.micromeso.2017.02.052
4. Al-Jumaily HAA. Qualitative Assessment of Pollution Indices for Heavy Metal of The Drinking Water in Kirkuk City, Northern Iraq. 2016;6(9). [Online].
Available: www.iiste.org
5. Adegoke HI, Adekola FA, Olowookere IT, Yaqub AL, Thermodynamic studies on adsorption of lead (II) Ion from aqueous solution using magnetite, activated carbon and composites, Journal of Applied Sciences and Environmental Management. 2017;21(3):440.

DOI: 10.4314/jasem.v21i3.5

6. Igwe JC, Abia AA, Ibeh CA, Adsorption kinetics and intraparticulate diffusivities of Hg, As and Pb ions on unmodified and thiolated coconut fiber, International Journal of Environmental Science and Technology. vol. 5, no. 1, pp. 83–92, 2008;5(1):83-92.
DOI: 10.1007/BF03326000
7. Agwaramgbo L, Lathan N, Edwards S, Nunez S. Assessing Lead Removal from Contaminated Water Using Solid Biomaterials: Charcoal, Coffee, Tea, Fishbone, and Caffeine, J Environ Prot (Irvine, Calif). 2013;4(7):741–745.
DOI: 10.4236/jep.2013.47085
8. Aksu Z, Akpinar D, Competitive biosorption of phenol and chromium(VI) from binary mixtures onto dried anaerobic activated sludge; 2001.
9. Monser L, Adhoum N, Modified activated carbon for the removal of copper, zinc, chromium and cyanide from wastewater ;2002. [Online].
Available: www.elsevier.com
10. Ho S, Removal of Dyes from Wastewater by Adsorption onto Activated Carbon: Mini Review," Journal of Geoscience and Environment Protection. 2020;08(05):120-131.
DOI: 10.4236/gep.2020.85008
11. Abdus-Salam N, Itiola AD, Potential application of termite mound for adsorption and removal of Pb(II) from aqueous solutions, Journal of the Iranian Chemical Society . 2012;9(3):373-382.
DOI: 10.1007/s13738-011-0047-2
12. Emeka C. Osakwe il Sanni S, Sa, Zubairu A, Adsorption of heavy metals from wastewaters using adonosia digitata fruit shells and theobroma cacao pods as adsorbents: A Comparative Study; 2014.
13. Alhamed YA, Bamufleh HS, Sulfur removal from model diesel fuel using granular activated carbon from dates' stones activated by ZnCl2, Fuel. 2009;88(1):87–94.
DOI: 10.1016/j.fuel.2008.07.019
14. Abdus-Salam N, Magaji B, Adsorption of Alizarin and Fluorescein Dyes on Adsorbent prepared from Mango Seed; 2014. [Online].
Available:https://www.researchgate.net/publication/263084358
15. Allahdin O, Foto E, Poumayé N, Biteman O, Mabingui J, Wartel M, Modeling of fixed bed adsorption column parameters of iron(ii) removal using ferrihydrite coated brick, Am J Analyt Chem. 2023;14(4):184–201
DOI: 10.4236/ajac.2023.144011
16. Gueu S, Yao B, Adouby K, Ado G, Kinetics and thermodynamics study of lead adsorption on to activated carbons from coconut and seed hull of the palm tree. Int. J. Environ. Sci. Tech. 2007;4(1):11-17.
17. Nsi EW, Akpakpan AE, Ukpong EJ, Akpabio UD, Preparation and characterization of activated carbon from hura crepitans linn seed shells.[Online].
Available: www.theijes.com
18. Ahmed Kabbashi N, Mirghani MES, Bello I, Md AZ, sam Yassin Qudsieh, Adebayo Bello I, Characterization of the Baobab fruit shells as adsorption material Ionic Liquids and / or Deep Eutectic Solvents View project Unconventional sources of vegetable oils View project Characterization Of The Baobab Fruit Shells As Adsorption Material Abstract; 2017.
19. Aksu Z, Tunç Ö, Application of biosorption for penicillin G removal: Comparison with activated carbon. Process Biochemistry. 2005;40(2):831–847.
DOI: 10.1016/j.procbio.2004.02.014.
20. Pavasant P, Apiratikul R, Sungkhum V, Suthiparinyanont P, Wattanachira S, Marhaba TF, Biosorption of Cu2+, Cd2+, Pb2+, and Zn2+ using dried marine green macroalga Caulerpa lentillifera, Bioresour Technol. 2006;97(18):2321–2329.
DOI: 10.1016/j.biortech.2005.10.032
21. Kamsonlian S, Balomajumder C, Suresh S, Majumder CB, Chand S, characterization of banana and orange peels:biosorption mechanism characterization of banana and orange peels: biosorption mechanism, International Journal of Science Technology & Management; 2011. [Online].
Available: www.ijstm.com
22. Weber (Jnr) JC, WJ, Morris, Equilbria and capacities for absorption of carbon. Journal of the Sanitary Engineering Division, Proceedings of the American Society of Civil Engineers. 1964;90:179–187.
23. Ugbe FA, Pam AA, Ikudayisi AV, Thermodynamic properties of chromium (III) ion adsorption by sweet orange (<i>Citrus sinensis</i>) Peels, Am J Analyt Chem. 2014;05(10): 666–673.
DOI: 10.4236/ajac.2014.510074

24. Mousavi HZ, Hosseinifar A, Jahed V, Studies of the adsorption thermodynamics and kinetics of Cr(III) and Ni(II) removal by polyacrylamide, Journal of the Serbian Chemical Society. 201277(3):393–405 DOI: 10.2298/JSC110410172M
25. Irving Lanowix B, adsorption of gases on glass, mica, and platinum. The adsorption of gases on plane surfaces of glass, mica, and platinum." J. Am. Chem. Soc. Publication. 1918;40:(9):1361–1403. Available:https://doi.org/10.1021/ja02242a004
26. Yee N, Benning LG, Phoenix VR, Ferris FG, Characterization of metal-cyanobacteria sorption reactions: A Combined Macroscopic and Infrared Spectroscopic Investigation, Environ Sci Technol. 2004;38(3):775–782 DOI: 10.1021/es0346680
27. Freundlich HMF, Over the adsorption in solution, Journal of Physical Chemistry. 1906;57(385471):1100–1107
28. Jnr MH, Spiff AI. Equilibrium sorption study of Al 3+ , Co 2+ and Ag + in Aqueous Solutions by Fluted Pumpkin (Telfairia Occidentalis HOOK f) Waste Biomass; 2005. [Online]. Available: https://www.researchgate.net/publication/279895008
29. Piccin JS, Dotto GL, Pinto LAA, Adsorption isotherms and thermochemical data of FDandC RED N° 40 Binding by chitosan, Brazilian Journal of Chemical Engineering. 295–304 2011;28(2):295-304. DOI: 10.1590/S0104-66322011000200014
30. Elmorsi TM, Mohamed ZH, Shopak W, Ismaiel AM, Kinetic and Equilibrium Isotherms Studies of Adsorption of Pb(II) from Water onto Natural Adsorbent, J Environ Prot (Irvine, Calif). 2014;5(17):1667–1681 DOI: 10.4236/jep.2014.517157
31. Ho YS, Mckay G, Pseudo-second order model for sorption processes; 1999.
32. Lagergren S, Zur theorie der sogenannten adsorption geloster stoffe, Kungliga Svenska Vetenskapsakademiens.Handlingar.1898;24.
33. Alzaydien AS. Manasreh W, Equilibrium, kinetic and thermodynamic studies on the adsorption of phenol onto activated phosphate rock; 2009. [Online]. Available: http://www.academicjournals.org/IJPS
34. Yakout SM, Elsherif E, Batch kinetics, isotherm and thermodynamic studies of adsorption of strontium from aqueous solutions onto low cost rice-straw based carbons; 2010. [Online]. Available: http://www.applied-science-innovations.com
35. Bhattacharyya KG, Sarma A, Adsorption characteristics of the dye, Brilliant Green, on Neem leaf powder, Dyes and Pigments. 2003;57(3):211–222. DOI: 10.1016/S0143-7208(03)00009-3
36. Shavandi MA, Haddadian Z, Ismail MHS, Abdullah N., "Continuous metal and residual oil removal from palm oil mill effluent using natural zeolite-packed column," J Taiwan Inst Chem Eng. 2012;43(6):934–941. DOI: 10.1016/j.jtice.2012.07.001
37. S.PS, CHAYANDE MKNYPK, Characterization of activated carbon prepared from almond shells for scavenging phenolic pollutants, Chem Sci Trans ; 2013. DOI: 10.7598/cst2013.358
38. Online R, Jiwalak N, Rattanaphani S, Bremner JB, Rattanaphani V, Equilibrium and kinetic modeling of the adsorption of indigo carmine onto Equilibrium and kinetic modeling of the adsorption of indigo carmine onto silk silk; 2010. [Online]. Available:https://ro.uow.edu.au/scipapers/425
39. Uddin MT, Abedin MZ, Uddin MT, Abedin MZ., Adsorption of phenol from aqueous solution by water hyacinth ash cryogenic composite fuel tanks view project Rehabilitation of oil and gas pipelines-Overwrap repairs View project Adsorption Of Phenol From Aqueous Solution By Water Hyacinth Ash," 2007;2(2). [Online]. Available: www.arpnjournals.com
40. Abechi SE, Studies on the mechanism of adsorption of methylene blue onto activated carbon using thermodynamic tools, Science World Journal, 2018;13(2). [Online]. Available: www.scienceworldjournal.org
41. Ketcha JM, DJD. Dina Ngomo HM, Ndi NJ, Preparation and Characterization of Activated Carbons Obtained from Maize Cobs by Zinc Chloride Activation; 2012. [Online]. Available: www.sciencedomain.org
42. Raffiea Baseri J, Palanisamy PN, Sivakumar P, Preparation and characterization of activated carbon from

Thevetia peruviana for the removal of dyes from textile waste water, Pelagia Research Library Advances in Applied Science Research. 2012;1:377–383 [Online]. Available: www.pelagiaresearchlibrary.com

43. Malik R, Ramteke DS, Wate SR, Adsorption of malachite green on groundnut shell waste based powdered activated carbon, Waste Management. 2007;27(9):1129–1138. ,
DOI: 10.1016/j.wasman.2006.06.009.
44. Ioannidou O, Zabaniotou A, Agricultural residues as precursors for activated carbon production-A review, Renewable and Sustainable Energy Reviews. 2007;11(9):1966–2005,
DOI: 10.1016/j.rser.2006.03.013
45. Bansode RR, Losso JN, Marshall WE, Rao RM, Portier RJ, Adsorption of metal ions by pecan shell-based granular activated carbons, Bioresour Technol. 2003;89(2): 115–119, ,
DOI: 10.1016/S0960-8524(03)00064-6
46. Vijayakumar G, Tamilarasan R, Dharmendirakumar M, Adsorption, Kinetic, equilibrium and Thermodynamic studies on the removal of basic dye Rhodamine-B from aqueous solution by the use of natural adsorbent perlite," J. Mater. Environ. Sci, 2011;3(1):157–170.
47. Satyawali Y. Balakrishnan M, Removal of color from biomethanated distillery spentwash by treatment with activated carbons," Bioresour Technol, 2007;98(14): 2629–2635, Oct.,
DOI: 10.1016/j.biortech.2006.09.016
48. Simonescu CM, Ferdes M, Fungal Biomass for Cu(II) Uptake from Aqueous Systems Innovative technologies for irrigation of agricultural crops in arid, semiarid and subhumid-dry climate (acronym: SMARTIRRIG) / Project 4: Innovative technological solution for capitalization of wastewater for irrigation of energy crops View project Environmental aspects on Romanian depressions View project ; 2012. [Online].
Available:https://www.researchgate.net/publication/258582904
49. Ahmedna M, Marshall WE, Rao RM., Production of granular activated carbons from select agricultural by-products and evaluation of their physical, chemical and adsorption properties q."
50. Fuat A, Pali A, Hungin S, Murphy JJ, Primary care Barriers to accurate diagnosis and effective management of heart failure in primary care: Qualitative Study.
51. Othman FEC. et al. Activated carbon nanofibers incorporated metal oxides for CO2adsorption: Effects of different type of metal oxides, Journal of CO2 Utilization. 2021;45
DOI: 10.1016/j.jcou.2021.101434
52. Khan TA, Khan TA, Ali I, Singh V, Sharma S, "As(V) removal capacity of various agricultural wastes View project Mechanism of retention and enantioseparation of chiral quinolones on enantioseparation of chiral quinolones on enantioselective adsorbents under liquid chromatographic conditions View project Utilization of Fly ash as Low-Cost Adsorbent for the Removal of Methylene Blue, Malachite Green and Rhodamine B Dyes from Textile Wastewater; 2009. [Online].
Available:https://www.researchgate.net/publication/228482268
53. Chen G. *et al.*, "Cadmium removal from simulated wastewater to biomass byproduct of Lentinus edodes. Bioresour Technol. 2008;99(15) 7034–7040
DOI: 10.1016/j.biortech.2008.01.020
54. Bhatia AK, Khan F, Biosorptive removal of copper (II) ion from Aqueous Solution using Lawsonia Inermis Plant Leaf Biomass. 2015;5(5). [Online]. Available: www.iiste.org
55. Burnett PGG, Daughney CJ, Peak D, Cd adsorption onto Anoxybacillus flavithermus: Surface complexation modeling and spectroscopic investigations, Geochim Cosmochim Acta. 2006;70(21): 5253–5269,
DOI: 10.1016/j.gca.2006.08.002
56. Hofmeister AM, Keppel E, Speck AK, Absorption and reflection infrared spectra of MgO and other diatomic compounds; 2003.
57. Akar E, Altinişik A, Seki Y, Using of activated carbon produced from spent tea leaves for the removal of malachite green from aqueous solution, Ecol Eng. 2013;52:19–27
DOI: 10.1016/j.ecoleng.2012.12.032
58. Baccar R, Bouzid J, Feki MA. Montiel, Preparation of activated carbon from Tunisian olive-waste cakes and its application for adsorption of heavy metal ions," J Hazard Mater. 2009;162(n2–3): 1522–1529, Mar.,

DOI: 10.1016/j.jhazmat.2008.06.041
59. Hesas RH, Arami-Niya, Wan Daud AWMA, Sahu JN, Preparation and characterization of activated carbon from apple waste by microwave-assisted phosphoric acid activation: Application in methylene blue adsorption, Bioresources. 2013;8(2):2950–2966
DOI: 10.15376/biores.8.2.2950-2966
60. Mohammadi T, Moheb AM, Sadrzadeh, Razmi A. Modeling of metal ion removal from wastewater by electrodialysis. Sep Purif Technol. 2005;41(1):73–82
DOI: 10.1016/j.seppur.2004.04.007
61. Elaigwu SE, Usman LA, Awolola GV, Adebayo GB, Ajayi RMK, Adsorption of Pb(II) from Aqueous Solution by Activated Carbon Prepared from Cow Dung," Advances in Natural and Applied Sciences. 2009;3(3):442–446,.
62. Nü L Dö Nmez G, Mriye Aksu Z, Removal of chromium(VI) from saline wastewaters by Dunaliella species." [Online].
Available:www.elsevier.com/locate/procbio
63. Ladhe UV, SK, Wankhede VT, Patil PR. Patil, Removal of erichrome black T from synthetic wastewater by cotton waste," *E*-Journal of Chemistry. 2011;8(2): 803–808
DOI: 10.1155/2011/178607
64. Arivoli S, Thiru Vi Ka, Arivoli S, Nandhakumar V, Saravanan S, Nagarajan S., Adsorption dynamics of copper ion by low cost activated carbon adsorption dynamics of copper ion by low cost activated carbon adsorption dynamics of copper ion by low cost activated carbon; 2008. [Online].
Available:https://www.researchgate.net/publication/242291799
65. Sanghi R, Bhattacharya B, Adsorption-coagulation for the decolorisation of Textile Dye Solutions; 2003. [Online].
Available:https://iwaponline.com/wqrj/article-pdf/38/3/553/229041/wqrjc0380553.pdf
66. Karthikeyan T, Rajgopal S, Miranda LR, "Chromium(VI) adsorption from aqueous solution by Hevea Brasilinesis sawdust activated carbon," J Hazard Mater. 2005:124(1–3):192–199,
DOI: 10.1016/j.jhazmat.2005.05.003
67. Tang D, Zheng Z, Lin K, Luan J, Zhang J, Adsorption of p-nitrophenol from aqueous solutions onto activated carbon fiber, J Hazard Mater. 2007:143:1–2:49–56.
DOI: 10.1016/j.jhazmat.2006.08.066
68. Das B., Mondal NK, Roy P, Chattaraj S, Equilibrium, Kinetic and Thermodynamic Study on Chromium(VI) Removal from Aqueous Solution Using Pistia Stratiotes Biomass, Chem Sci Trans. vol. 2012; 2(1):85–104,
DOI: 10.7598/cst2013.318
69. Mekonnen E, Yitbarek M, Soreta TR, Kinetic and thermodynamic studies of the adsorption of Cr(VI) onto some selected local adsorbents, South African Journal of Chemistry. 2015;68:45–52
DOI: 10.17159/0379-4350/2015/v68a7
70. Shukla A, Zhang YH, Dubey P, Margrave JL, Shukla SS. The role of sawdust in the removal of unwanted materials from water; 2002.
71. Jimoh TO, Yisa J. Ajai AI, Musa A, Kinetics and Thermodynamics Studies of the Biosorption of Pb(II), Cd(II) and Zn(II) Ions from Aqueous Solution by Sweet Orange (Citrus sinensis) Seeds," International Journal of Modern Chemistry Int. J. Modern Chem. vol. 2013;4(1):19–37. [Online].
Available:www.ModernScientificPress.com/Journals/IJMChem.aspx
72. Cheng Q. et al., Adsorption of Cd by peanut husks and peanut husk biochar from aqueous solutions. Ecol Eng. 2016; 87:240–245.
DOI: 10.1016/j.ecoleng.2015.11.045
73. Asiagwu AK, Sorption kinetics of Pb (II) and Cd (II) ions via biomass surface of plantain peel waste; 2012. [Online].
Available:www.arpapress.com/Volumes/Vol13Issue2/IJRRAS_13_2_29.pdf
74. G Atun, Tunçay M, Hisarli GRY. Talman, H. Hoşgörmez, Adsorption equilibria between dye and surfactant in single and binary systems onto geological materials," Appl Clay Sci. 2009;45(4): 254–261.
DOI: 10.1016/j.clay.2009.06.003
75. Goel J, Kadirvelu K, Rajagopal C, Garg VK, Removal of lead(II) by adsorption using treated granular activated carbon: Batch and column studies," J Hazard Mater. 2005;125(1-3):211–220
DOI: 10.1016/j.jhazmat.2005.05.032.
76. Meunier N, Laroulandie J, Blais JF, Tyagi RD, Cocoa shells for heavy metal removal from acidic solutions, Bioresour Technol. 2003;90(3):255–263
DOI: 10.1016/S0960-8524(03)00129-9
77. Sari A, Tuzen M, Soylak M, Adsorption of Pb(II) and Cr(III) from aqueous solution on

Celtek clay, J Hazard Mater. 2007;144(1–2):41–46, May,
DOI: 10.1016/j.jhazmat.2006.09.080

78. Conrad K, Bruun HC, Hansen, "Sorption of zinc and lead on coir," Bioresour Technol. 2007;98(1):89–97.
DOI: 10.1016/j.biortech.2005.11.018
79. Xiyili H, Çetintaş S, Bingöl D, Removal of some heavy metals onto mechanically activated fly ash: Modeling approach for optimization, isotherms, kinetics and thermodynamics, Process Safety and Environmental Protection. 2017;109:288–300.
DOI: 10.1016/j.psep.2017.04.012
80. Pan X, Zhang D., Removal of malachite green from water by Firmiana simplex wood fiber, Electronic Journal of Biotechnology. 2009;12(4).
DOI: 10.2225/vol12-issue4-fulltext-4
81. Debnath S, Ghosh UC, Kinetics, isotherm and thermodynamics for Cr(III) and Cr(VI) adsorption from aqueous solutions by crystalline hydrous titanium oxide," Journal of Chemical Thermodynamics. vol. 2008;40(1):67–77
DOI: 10.1016/j.jct.2007.05.014
82. Helfferich F, Ion-Exchange. Adelaide, Australia: New York: Mc Graw-Hill; 1962.
83. Nassar NN, Rapid removal and recovery of Pb(II) from wastewater by magnetic nano-adsorbents," J Hazard Mater. 2010;184(1–3):538–546
DOI: 10.1016/j.jhazmat.2010.08.069
84. Nebagha KC. *et al*, Adsorptive removal of copper (II) from aqueous solutions using low cost Moroccan adsorbent. Part I: Parameters influencing Cu(II) adsorption," J. Mater. Environ. Sci. 2015;6(11):3022–3033
85. Suhaida A, Naspu M, Lias Kamal M, Hasan S., "Adsorption-Desorption Study of Metal Ions on Brown Macro Algae Padina sp, Journal of Applied Science and Agriculture. 2014;9(11):1–8, [Online]. Available: www.aensiweb.com/JASA
86. Lai FY, Lin YP, Lu C. Effects of carbonization temperature on phytochemicals and antioxidant activities of "cabbage-like" vegetable juices. Journal of Food and Drug Analysis. 2017;25(4): 842-848.
DOI: 10.1016/j.jfda.2016.10.010
87. Sun J, Liu J, Liu B, Zhu X, Xu X. Effects of carbonization temperature on characterization of activated carbons prepared from apricot shells and their application in methylene blue adsorption. Applied Surface Science. 2018;427(Part A):676-682
DOI: 10.1016/j.apsusc.2017.08.190
88. Abubakar E, Ismat H. Ali, Eid I. Brima, A. B. Elhag and Babiker K. Efficient Removal of Ni(II) from Aqueous Solution by Date Seeds Powder Biosorbent: Adsorption Kinetics, Isotherm and Thermodynamics. Processes 2020;8:1001; DOI:10.3390/pr8081001
89. Ma L, Qi W, Liu S, Zhang T, Zhang L, Mei M, Zheng T. Preparation and characterization of activated carbon derived from walnut shell as an adsorbent for heavy metal removal. Journal of Environmental Chemical Engineering. 2019;7(2); 102954.
90. Huang W, Xing S, Wang Y, Kong X, Li J, He H, Zhou Y. Magnetic graphene oxide-based nanocomposites: preparation, adsorption properties, and photocatalytic degradation of pollutants. ACS Applied Materials & Interfaces. 2015;7(11):6121-6131.
91. Shukla A, Zhang YH, Dubey P. Margrave JL, Shukla SS. The role of sawdust in the removal of unwanted materials from water. Journal of Hazardous Materials. 2002;95(1-2):137-152.
92. Foo KY, Hameed BH Insights into the modelling of adsorption isotherm systems. Chemical Engineering Journal. 2010;156(1):2-10.
93. Kumar E, Bhatnagar A, Han B. Thermodynamics and kinetics of arsenic adsorption onto iron oxide-based adsorbents. Journal of Hazardous Materials, 2008;156(1-3):407-416.

Peer-review history:
The peer review history for this paper can be accessed here:
https://www.sdiarticle5.com/review-history/107181